

DESIGN, DEVELOPMENT, AND EXECUTION OF PIV MEASUREMENTS ON A
RANDOMLY PACKED PEBBLE BED EXPERIMENTAL FACILITY USING
MATCHED INDEX OF REFRACTION

A Thesis

by

ETHAN DANIEL KAPPES

Submitted to the Office of Graduate and Professional Studies of
Texas A&M University
in partial fulfillment of the requirements for the degree of

MASTER OF SCIENCE

Chair of Committee,	Yassin A. Hassan
Committee Members,	Rodolfo Vaghetto
	Maria King
Head of Department,	Yassin A. Hassan

December 2018

Major Subject: Nuclear Engineering

Copyright 2018 Ethan Daniel Kappes

ABSTRACT

Randomly packed pebble bed structures are found in many engineering applications, such as solar thermal batteries, chemical catalytic reactors, fluid refinement and filtering, magnetic refrigerators, biological tissues, and pebble bed reactors. The critical challenge of designing and analyzing a packed bed structure especially in the nuclear industry comes from its complex and dynamic geometry. Modeling and understanding the complex flow, heat and mass transfer, and vorticity phenomena within the bed on a micro scale involves in-depth analysis of the interstitial regions that make up its entirety. Unfortunately, complex geometries and randomly connected void spaces within packed beds have hindered efforts to characterize the underlying transport phenomena.

Current research lacks analysis and validation against accurate computational fluid dynamics models for randomly packed structures. This lack of understanding prevents proper leveraging of the pebble bed reactor's passive safety features. Current PIV research that involves randomly packed structures does not also provide a 3-Dimensional (3D) replica of the test bed for verification. Noninvasive measurements coupled with a full 3D test bed replica for computational fluid dynamic verification and validation will lead to a full understanding of the microscopic flow phenomena within pebble bed reactors.

Texas A&M University is conducting isothermal experiments of pressure drops, and flow analysis in a randomly packed pebble bed experimental facility to support the research on advanced nuclear reactors. The data collected is expected to be suitable for computational fluid dynamics validation. The design, construction, and collection of shakedown pressure and PIV data with differing pebble to pipe diameter ratios were conducted in efforts to provide needed data on local flow measurements. The use of nonintrusive PIV analysis on a randomly matched

index of refraction facility. This approach allows for a non-invasive probe into the flow within packed spheres at the microscopic scales with high temporal and spatial resolutions. Effects of the wall boundary and Reynolds on flow characteristics obtained from the TR-PIV measurements with are presented with high spatial and temporal resolution.

ACKNOWLEDGEMENTS

This research and my degree would not have been possible without the support I received during my time here. Trials inside the laboratory, the classroom, my home, and my personal life have been more abundant now than ever before. I would like to thank my family, for always being by my side and giving me the advice gained through their years of experience. My friends in the lab, my friends in my classes, and my undergraduate team. for all their support and help with the problems I faced during my time here. My professors for preparing me for this endeavor.

I would like to personally thank Dr. Yassin A. Hassan for his continued guidance and understanding during my time here at Texas A&M. You have been an amazing advisor a true friend and a caring teacher. Thank you for your time and care.

I would also like to thank Dr. Thien Nguyen. You have always offered me your help and taught me what this research meant. You stood by my side and showed me what it was to work in the laboratory. I would without a doubt be lost without the help you provided, and your insight into the complexities of our research. I can never thank you enough for being a great mentor and friend.

CONTRIBUTORS AND FUNDING SOURCES

Contributors

The work completed for this experimental research was supervised by a committee consisting of Dr. Yassin A. Hassan and Dr. Rodolfo Vaghetto of the Nuclear Engineering Department, and Dr. Maria King of the Mechanical Engineering Department of Texas A&M University.

All work was completed under the advisement and supervision of Dr. Yassin A. Hassan, Dr. Rodolfo Vaghetto, and Dr. Thien Nguyen of the Department of Nuclear Engineering.

Funding Sources

This research is financially supported by the U.S. Department of Energy (DOE), NEAMS project and under a contract [DE-NE0008550]. Funding sources were part of an NEUP grant with contributors such as the U.S. DOE, Argonne National Lab (ANL), Xenergy, and the Institut "Jožef Stefan".

NOMENCLATURE

2D2C	Two-Dimensional Two Component
3D	3 Dimensional
AHTR	Advanced High-Temperature Reactor
ANL	Argonne National Laboratory
AVR	Arbeitsgemeinschaft Versuchsreaktor
CAD	Computer-Aided Design
CFD	computational fluid dynamics
D/d_p	pipe-to-pebble aspect ratio
DAS	data acquisition system
DOE	U.S. Department of Energy
FCC	Face Centered Cubic
GEN	Generation
HTGR	high temperature gas cooled reactor
LIF	Laser Induced Fluorescence
MIR	matched-index-of-refraction
MSR	Molten Salt Reactor
NEAMS	Nuclear Energy Advanced Modeling and Simulation
NEUP	Nuclear Energy University Program
PBR	pebble bed reactor
PIV	particle image velocimetry
PMMA	Poly (methyl methacrylate)
PTFE	Polytetrafluoroethylene

PVC polyvinyl chloride

Re Reynolds

RMS root-mean-square

ROI region of interest

SPIV stereoscopic particle image velocimetry

SS stainless steel

TAMU Texas A&M University

TR-PIV Time-Resolved Particle Imaging Velocimetry

UHMWPE ultra-high-molecular-weight polyethylene

VFD variable frequency drive

TABLE OF CONTENTS

	Page
ABSTRACT.....	ii
ACKNOWLEDGEMENTS	iv
CONTRIBUTORS AND FUNDING SOURCES	v
NOMENCLATURE	vi
TABLE OF CONTENTS.....	viii
LIST OF FIGURES	x
LIST OF TABLES.....	xii
1 INTRODUCTION.....	1
2 OBJECTIVES.....	6
2.1 Primary Proposal	6
2.1.1 Objective 1: Particle Image Velocimetry (PIV).....	6
2.1.2 Objective 2: Internal Thermal Profiles.....	7
2.1.3 Objective 3: Computational Simulation.....	8
3 LITERATURE REVIEW	10
3.1 Pebble Bed Flow Characterization and Scaling	10
3.2 Matched-Index-of-Refractive Facilities.....	13
4 PRESSURE FACILITY DESIGN	14
4.1 Pressure Test Section	14
5 MIR FACILITY DESIGN.....	17
5.1 Materials Selection.....	17
5.2 Test Section	20
5.2.1 Facility One	21

5.2.2	Facility Two	25
5.3	Leak Testing.....	25
5.4	Imaging hardware.....	26
5.4.1	PIV Setup and Hardware.....	26
6	FACILITY TWO TEST BED SCAN.....	30
7	PARTICLE IMAGING VELOCIMETRY	34
8	PIV RESULTS	38
9	CONCLUSION AND LESSONS LEARNED.....	46
	REFERENCES	47
	APPENDIX A. MIR FACILITY DRAWINGS	49
	APPENDIX B. PEBBLE CENTROID LOCATIONS LIST.....	66
	APPENDIX C. PEBBLE RECONSTRUCTION PHOTOS.....	70

LIST OF FIGURES

	Page
Figure 1.1: Example reactor with TRISO particle and core specifications [1].....	2
Figure 1.2: Project funding sources for NEUP grant.....	5
Figure 2.1: PIV/LIF experimental set-up.....	7
Figure 2.2: Preliminary computational simulation results.....	9
Figure 3.1: Radial porosity oscillations vs. Sphere diameter distance from inner wall [8].....	11
Figure 3.2: List of basic equations used when scaling facility and determining experimental parameters.....	12
Figure 4.1: Preliminary loop of experimental pressure drop facility created for correlation testing.....	14
Figure 4.2: Isometric view of pressure drop experimental facility with components labeled.....	15
Figure 4.3: Water pressure-drop data collected from primary pressure facility constructed Copyright (2017) by the American Nuclear Society, La Grange Park, Illinois [6].....	16
Figure 5.1: Small PMMA pipe filled with PMMA pebbles p-Cymene and air.....	19
Figure 5.2: Scaled pebbles next to ruler ranging from 31.75 mm to 12.7 mm.....	20
Figure 5.3: (a) Isometric over view of first facility, (b) facility filled with PMMA pebbles, and (c) photo of fresh p-Cymene filling test section.....	22
Figure 5.4: The hexagonal test section (left), reducer (middle), and square inlet pipe (right).....	24
Figure 5.5: Experimental facility fully installed (left) with square inlet tube base (right).....	25
Figure 5.6: Cad of experimental setup two.....	26
Figure 5.7: Experimental facility two.....	26

Figure 5.8: (a) Experimental setup of time-resolved PIV measurements, (b) front-view and cross section of the visualization section.....	27
Figure 5.9: Experimental test section during filled with air (left), p-Cymene (middle), and during operation (right)	28
Figure 5.10: Hexagonal (left) and square (right) sections during operation.....	28
Figure 5.11: Top down radial PIV through upper plenum of second facility.....	29
Figure 6.1: Test bed scan setup (left) with actual test bed scan image (right).....	30
Figure 6.2: Image pair used to verify reconstruction accuracy.....	32
Figure 6.3: 3D CAD experimental pebble bed reconstruction	33
Figure 7.1: Raw PIV images from top (left) and bottom (right) cameras during operation	35
Figure 7.2: Combined images from top and bottom cameras	36
Figure 8.1: Velocity vector and color contour of velocity magnitude TR-PIV results [14] reprinted with permission Copyright © 2018 by ASME.....	40
Figure 8.2: Velocity vector and color contour of z-vorticity results from TR-PIV measurements [14] reprinted with permission Copyright © 2018 by ASME	41
Figure 8.3: RMS results of fluctuating horizontal velocity (left), vertical velocity (middle), and Reynolds stress (right) from TR-PIV measurements [14] reprinted with permission Copyright © 2018 by ASME.....	42
Figure 8.4: Comparison of statistical results obtained by TR-PIV measurements on the MIR facility of packed spheres for $Re_1 = 340$ (red), $Re_2 = 520$ (green), and $Re_3 = 720$ (blue) [14] reprinted with permission Copyright © 2018 by ASME	44

LIST OF TABLES

	Page
Table 1.1: List of some specifications for PBR facilities	1
Table 5.1: Material selection used for the experimental facility	18
Table 5.2: Experimental test section one measurements	23
Table B.1: Centroid listing for spheres in experimental facility two.....	66
Table C.1: Image set of corresponding laser scans and 3D CAD cross sections.....	71

1 INTRODUCTION

Randomly packed pebble bed structures are found in many engineering applications, such as solar thermal batteries, chemical catalytic reactors, fluid refinement and filtering, magnetic refrigerators, biological tissues, and Pebble Bed Reactors (PBR). The critical challenge of designing and analyzing a packed bed structure especially in the nuclear industry comes from its complex and dynamic geometry. Modeling and understanding the flow, heat and mass transfer, and vorticity phenomena within the bed on a micro scale involves in-depth analysis of the interstitial regions that make up its entirety. Unfortunately, complex geometries and randomly connected void spaces within packed beds have hindered efforts to characterize the underlying transport phenomena. The high efficiency of the PBR has led to an increased interest in the Generation IV (GEN IV) design. Table 1.1 lists some notable specifications of the PBR designs that can be expected.

Table 1.1: List of some specifications for PBR facilities

Typical Parameters	
Thermal Output (MWth)	200 - 400
Coolant Type	He, FLiNaK, Other Molten Salts
Core Outlet Temperature (°C)	700 - 900
Core Diameter (m)	3 – 3.5
Sphere Diameters (mm)	30 - 60
Triso Microsphere Diameter (mm)	~ 1
Number of Pebbles	220,000 – 452,000

The Advanced High-Temperature Reactor (AHTR) concept leverages a particle-based fuel format consisting of discrete spherical graphite pebbles arrayed in a packed bed architecture. In the PBR, thermal regulation can be achieved via flow of gas (helium) or liquid (molten salt) as coolants through void spaces between pebbles in the bed. The increased efficiency and temperature coupled with the passive safety features of the PBR make it a prime candidate for power production, as well as process heat production. The PBR has the capability of using either Helium or Molten Salt for the coolant with 6 cm or 3 cm diameter fuel pebbles, respectively. An example of a High Temperature Gas-cooled Reactor (HTGR) PBR design can be seen in Figure 1.1.

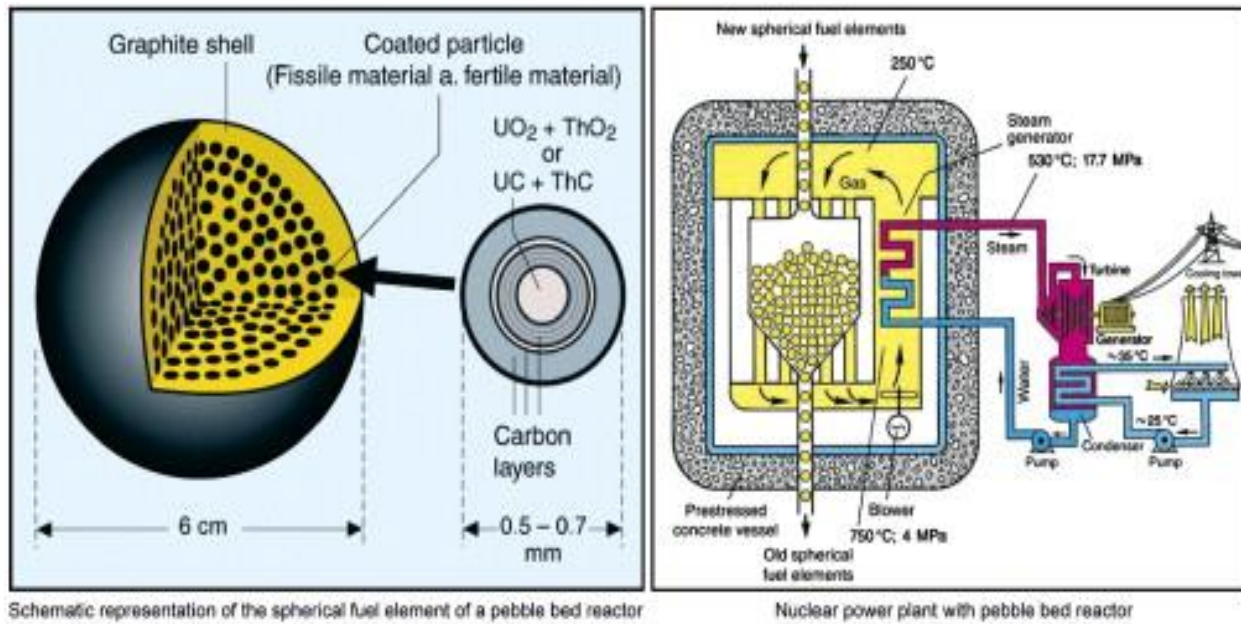


Figure 1.1: Example reactor with TRISO particle and core specifications [1]

Some of the most notable features of the PBR design are the ability to refuel during operation, dynamic geometry, high temperatures range, and the inability to melt down both during

normal operation and loss of coolant incidents. However, full utilization of the safety features of the PBR design require a fundamental understanding of the complex flow structures within the bed itself. The geometrical complexity inside of a PBR present a challenge to experimental and computational efforts. Transport models have previously built upon volume averages of micro-scale parameters; however, this does not accurately capture the flow behaviors. Simplified, symmetrically packed beds built for testing results are far from realistic without considering the random and shifting packing structure.

The first PBR design, the Arbeitsgemeinschaft Versuchsreaktor (AVR), was brought online in 1967. This test reactor ran from 1967 to 1988 when it was decommissioned after a radioactive release. This failure was due to a lack of understanding of localized areas within the reactor, mainly microscopic regions in the fuel bed. This led to hot zones, subjecting spheres to beyond-operating-condition temperatures. These extreme temperatures, coupled with constant shifting and poorly fabricated test spheres, caused the degradation of fuel pebbles and heavily contaminated the reactor vessel with ^{90}Sr .

Study of the PBR's microscopic-level measurements and bypass-flow analysis in the fuel bed can lead to a full understanding the flow phenomena on the pore level. Bypass flow in the near wall regions has an oscillating effect on the porosity which also causes high temperature variations due to lack or increase of heat removal. The lack of understanding and data in these areas has created a demand for experiments to investigate the wall effects on the pressure, flow, and heat removal capabilities of these systems. Arthur et al [2] varied boundary conditions in porous media to study three boundary conditions with varying solid volume fraction. Khayamyan and Lundstrom [3] studied transitional flow (i.e., flow between the laminar and turbulent flow regimes) in porous media along with pressure-drop calculations. Hassan and Kang [4] performed pressure-drop

measurements for a packed bed design with varying packing factors under high Reynolds (Re) number. Patil and Liburdy [5] performed detailed flow measurements in a randomly packed bed of spheres using Particle Imaging Velocimetry (PIV) technique.

Texas A&M University (TAMU) is therefore conducting isothermal and non-isothermal measurements of pressure drop, flow, and heat transfer in a pebble bed experimental facility to support the research on advanced nuclear reactors sponsored by Department of Energy (DOE). Results of pressure-drop measurements were previously discussed in [6]. In this thesis, I present measurements of internal flow fields within an experimental facility of randomly packed bed of spheres that represents the core of a pebble bed reactor. This thesis met aspects of the demand for a more in-depth analysis of the pebble bed's structure and effect on flow. The experiments involved the creation of a facility to model the reactors core for pressure studies, and flow phenomena with a third facility in construction for heat and mass transfer phenomena measurements. This thesis will go into detail about the PIV studies done by combining an approach of Matched Index of Refraction (MIR) and Time-Resolved Particle Imaging Velocimetry (TR-PIV) technique.



Figure 1.2: Project funding sources for NEUP grant

This research is financially supported by the U.S. DOE, NEAMS project and under a contract [DE-NE0008550]. Funding sources were part of an NEUP grant with contributors such as the U.S. DOE, Argonne National Lab (ANL), Xenergy, and the Institut "Jožef Stefan".

2 OBJECTIVES

The main Objectives that were originally presented by TAMU in the experimental proposal can be found below. The objective met during the completion of this thesis was Objective 1 seen in Section 2.1.1.

2.1 Primary Proposal

2.1.1 Objective 1: Particle Image Velocimetry (PIV)

Perform in-situ velocity and temperature distribution measurements within a pebble bed flow system using state-of-the-art high-speed high-resolution PIV and Laser Induced Fluorescence (LIF) techniques. This data will help to create a better understanding of the fundamental interstitial flow phenomena, generating new data that is needed to rationally develop improved models capable of capturing these characteristics. The unique challenges associated with interrogating flow in the void spaces within the packed bed will be addressed by using a MIR technique. MIR enables any point within the test section to be optically accessible at any bed diameter. Advanced image processing techniques will be employed to obtain a three-dimensional reconstruction of the radial porosity distribution with high spatial resolution. Pressure-drop associated with flow through the bed will be measured at multiple locations to enable comparison against existing correlations in homogenous packed beds and suggest refinements to more accurately represent the pebble bed system. Confining wall effects and inhomogeneous porosity within the bed are examples of non-ideal factors we will consider that are not captured in existing model frameworks.

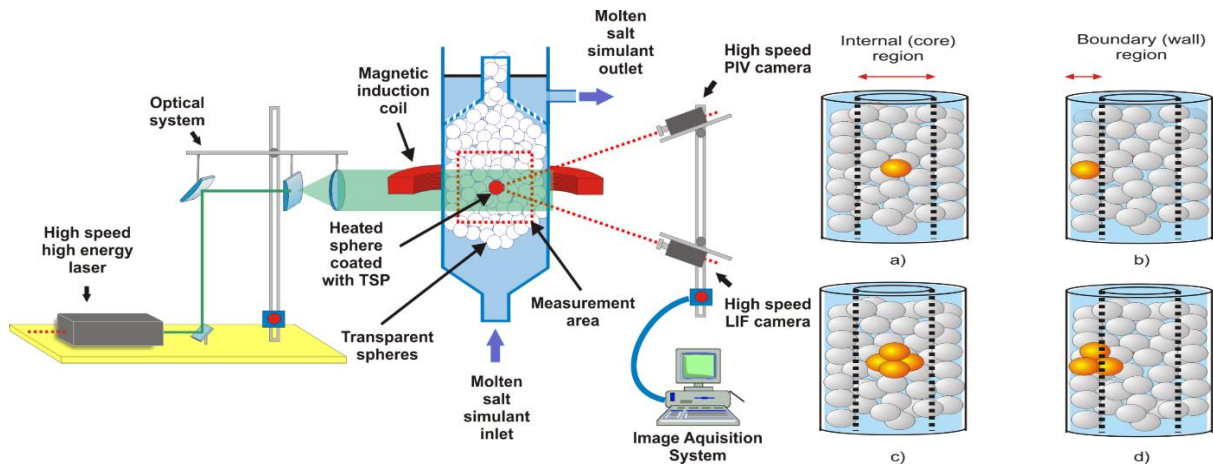


Figure 2.1: PIV/LIF experimental set-up

Figure 2.1 shows an example experimental setup for non-intrusive fluid flow and heat transfer measurements in a packed bed utilizing PIV, MIR, LIF, and Induction Heating. Right: (a), (b), (c) and (d) delineate locations of heated spheres within the bed.

2.1.2 Objective 2: Internal Thermal Profiles

Leveraging a unique magnetic induction heating system that permits selective heating of individual pebbles or clusters of pebbles inside the test section will be used to build on studied in Objective 1. These experiments will enable, for the first time, to directly probe effects associated with hot spots in the packed bed interior. This type of phenomena has not been extensively studied experimentally, despite the importance of obtaining accurate computational models of this scenario. Coordinated non-invasive LIF measurements in the fluid will also be performed using fluorescent tracers with different emission wavelengths. One species will display strong temperature dependence in the range of interest, while the second will serve as a control against run-to-run variations in illumination and detection conditions.

2.1.3 Objective 3: Computational Simulation

Leveraging the new experimental data obtained in Objectives 1 and 2, the computational component of this work will address the lack of modeling capability to accurately represent the multi-scales of flow and thermal transport in the interstitial pore spaces within the pebble bed. We will accomplish this by employing state-of-the-art Computational Fluid Dynamic (CFD) modeling to capture fine details associated with the velocity and temperature fields in these systems. These advancements will provide new inputs to improve and refine accuracy of NEAMS-capable simulation tools. Specifically, our CFD analysis efforts will be coordinated with a National Lab Partner engaged in development of relevant simulation tools (e.g., Nek5000) to ensure practical adaptation of these results. Our sensitive high-speed imaging capabilities will in turn provide the exciting capability to directly validate the results of these simulations and will allow us to directly observe the interplay between the flow field and temperature distribution within the pebble bed across a broad range of time and length scales (Figure 2.2).

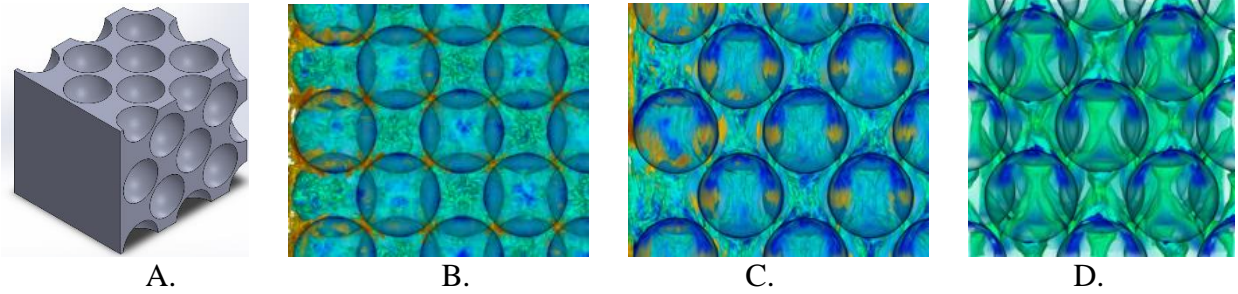


Figure 2.2: Preliminary computational simulation results

Figure 2.2 shows some preliminary results of interstitial flow within a pebble bed arrangement obtained in partnership with US National Laboratory collaborators. (a) Face Center Cubic (FCC) structured packed bed, with periodic boundaries and a single bounding wall. Instantaneous velocity profiles (b) parallel and (c) normal to the stream-wise direction reveal higher velocity bypass flow in the near wall region. (d) Averaged velocity profile normal to the stream-wise direction reveals local stagnation zones behind and ahead of the pebbles in the direction of the flow.

3 LITERATURE REVIEW

The literature review was performed to develop an understanding of the current research performed on pebble bed facilities. The review covers scaling analysis done as well as previous non-intrusive measurements applied to pebble beds for experimental facilities.

3.1 Pebble Bed Flow Characterization and Scaling

Dominguez and Hassan [7] were one of the first to perform localized investigations into pebble bed flow phenomena. These techniques enabled pore scale imaging within the pebble bed. The previous investigations of flow, heat transfer, and pressure drop were bulk investigations. These investigations left much to be desired especially in former categories. Flow and heat and mass transfer across the entire bed have been measured but this investigation took into consideration the microscale flow phenomena that occurred in randomly packed beds varying pipe-to-pebble aspect ratio (D/d_p) aspect ratios. This study involved a square channel with a randomly packed bed investigating flow phenomena within the interstitial regions. Therefore, a demand existed for a larger scale experiment with larger spheres and smaller aspect ratios for investigation into wall effects on bypass flows.

This thesis met those demands through the design, construction and data collection performed during the experiment. This bed involved the use of spheres equivalent to the size of those found in Molten Salt Reactor (MSR) pebble bed (3cm). These larger spheres and smaller aspect ratios would cause a much larger variation in porosity seen within the experimental facility allowing for a much more in-depth understanding of the flow phenomena. This greater variation in porosity and larger interrogation areas would give the opportunities to provide data over a more

diverse geometry. The magnitude of the oscillating porosity within the pebble bed is seen to lessen as more sphere diameters are added from the inner wall. The oscillations caused by wall effects can be seen in Figure 3.1 below as the left and right edges of the graph represent the pipe inner wall. The figure shows how the porosity reaches an average value from three to five diameters distance from the wall. It was determined that to state wall effects to be negligible in the bed a minimum of 50 sphere diameters across the entire pebble bed would be needed.

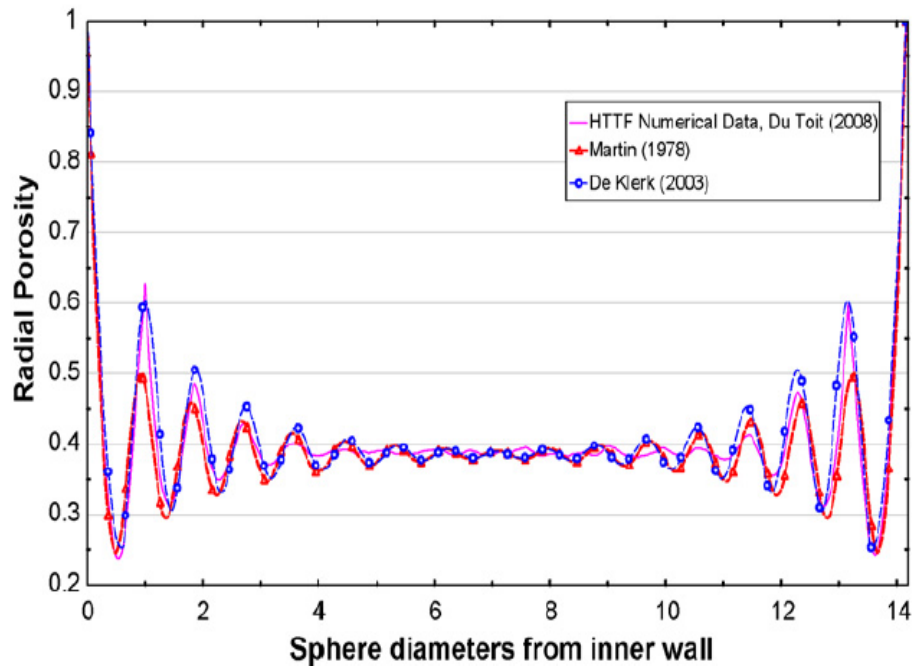


Figure 3.1: Radial porosity oscillations vs. Sphere diameter distance from inner wall [8]

Randomly packed beds such as pebble bed reactors have been determined to reach turbulent regimes at lower flow rates due to the complex geometry. The continuous mixing of the fluid is due to the winding pathways created by the void areas between the pebbles that direct the flow. These pathways rarely allow for developed laminar region within the pebble bed itself. Re

numbers fell within four categories according to Rahman Abdulmoshin [8]. Stating that the flow regimes for the adjusted Re number are Re_h .

- Effective Hydraulic Diameter: $d_h = d_p \frac{\varepsilon_b}{(1-\varepsilon_b)}$
- Mean Porosity: $\varepsilon_b = \frac{0.78}{(D/d_p)^2} + 0.375$
- Interstitial Velocity: $V = \frac{V_g}{\varepsilon_b}$
- Adjusted Reynolds number $Re_h = \frac{\rho V d_h}{\mu}$

Figure 3.2: List of basic equations used when scaling facility and determining experimental parameters.

Where ε_b is the average porosity of the packed bed a function of the D/d_p ratio that has multiple calculations for specific D/d_p values. The d_h , and V are the effective hydraulic diameter and interstitial velocity, respectively. These are averaged Re number calculations that must be applied to the entire bed as the porosity within will change constantly depending on the measurement location. The Re therefore is an average based on the porosity of the pebble bed and its porosity a function of the D/d_p ratio. Flow regimes were categorized as follows, creeping ($Re_h < 1$), steady laminar-flow ($1 < Re_h < 150$), unsteady laminar-flow ($150 < Re_h < 300$), and turbulent-flow ($Re_h > 300$).

Through the literature review [9] it was determined that the primary scaling parameter for flow mechanics within the pebble bed itself would be the aspect ratio D/d_p . The basic structure of the facility would therefore be simple. Constructing a facility to be used for PIV using MIR without the use of correction boxes for the imaging technique to be applied was a main concern. Restricting

measurements to the single-phase flow phenomena simplified the scaling parameters to the Re number, D/d_p , and the flow regimes planned to be observed.

3.2 Matched-Index-of-Refractive-Index Facilities

Previous studies were performed using solids and fluids in order to create MIR facilities. Prior work at TAMU in the Thermal-Hydraulic Research Laboratory has investigated and used multiple fluid/solid pairs. Dominguez and Hassan [7] performed a study involving determination of a working fluid and solid that could be used for a MIR pebble bed facility. After optical testing, they selected PMMA for the facility and p-Cymene for the working fluid.

These materials were determined to be the best choice for cost effectiveness and current availability. The facility's unique design also allowed for the use of a single test section with no adhesives and no correction box needed. This facility also created opportunities for Stereoscopic Particle Imaging Velocimetry (SPIV). The second experimental facility setup allowed for a 3D reconstruction of the randomly packed bed of a studied section of the pebble bed.

4 PRESSURE FACILITY DESIGN

During this research three facilities were designed each with the capability of exchanging pebble sizes for different D/d_p aspect ratios. The first was an experimental facility specifically used for pressure drop as a proof of concept and can be seen in Figure 4.1.

The isometric view of the solid works design with labeled components in Figure 4.2 shows the final build that would involve the use of the primary pump. The pressure facility incorporated pressure ports both within the bed and across the full length of the bed as well as the ability to perform both gas and liquid pressure-drop measurements. The pressure facility has produced correlative data using both liquid and gas flow under the supervision of Stephen King and can be seen here [6].

4.1 Pressure Test Section

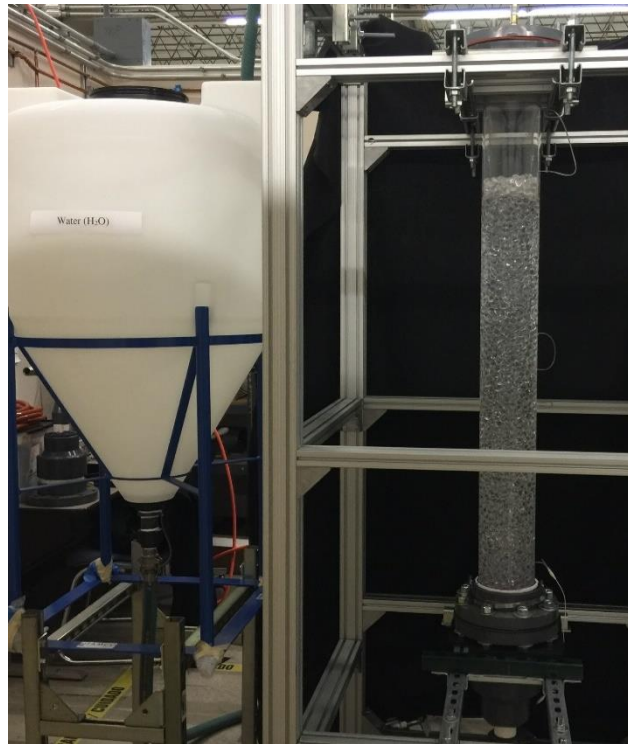


Figure 4.1: Preliminary loop of experimental pressure drop facility created for correlation testing

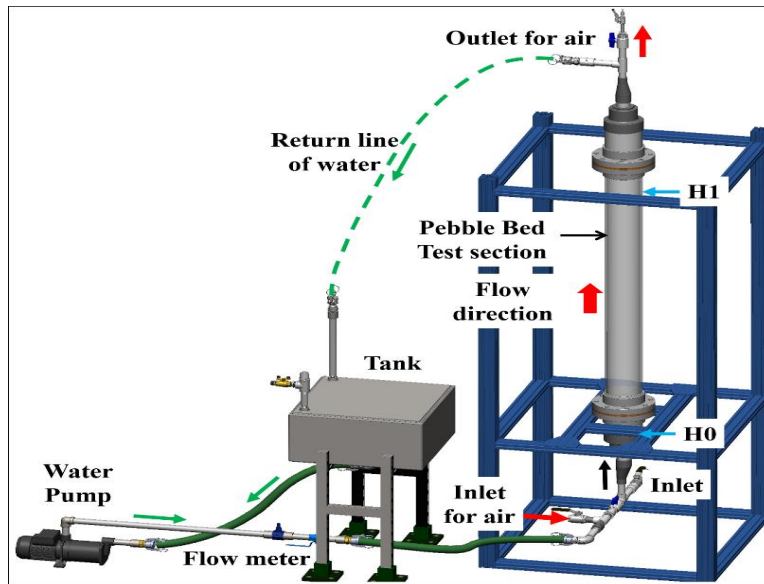


Figure 4.2: Isometric view of pressure drop experimental facility with components labeled

Pressure drops associated with flow through the bed were to be measured at multiple locations to enable comparison against existing correlations in homogenous packed beds and suggest refinements to more accurately represent the pebble bed system. Due to obstructions at the ports and varying of interstitial velocities because of the porosity changes. The data was collected only as a bulk measurement and cross referenced with other correlations already performed on pebble bed facilities data collected and analyzed by Stephen King can be seen below in Figure 4.3. Results obtained from this experimental section were done in conjunction with the completion of this thesis, but will not be presented within this paper.

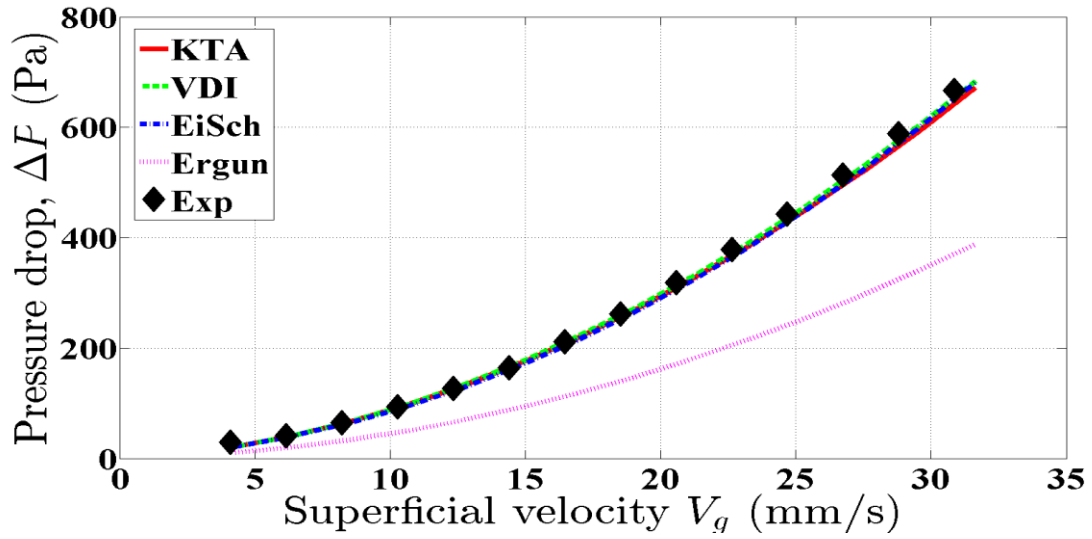


Figure 4.3: Water pressure-drop data collected from primary pressure facility constructed
 Copyright (2017) by the American Nuclear Society, La Grange Park, Illinois [6]

5 MIR FACILITY DESIGN

To complete the objectives outlined by the proposal seen in Section 2.1 a MIR facility was required. The MIR facility involved the use solid/fluid pairs with refractive indices that are similar enough to provide optical clarity and mechanical strength. The TAMU Thermal-Hydraulics Laboratory is well versed in the design, development, and execution of MIR facility builds. Previous knowledge from the Thermal-Hydraulic Laboratory had a large impact on the selection of materials and the design of the facility. The facilities main components were the upper plenum, hexagonal pipe test section, square inlet pipe, reducer, diffuser, perforated steel plates, reservoir tank, pump, and chemical hosing.

The materials selection for the facility was based mainly on the previous MIR and PIV studies performed by the TAMU Thermal-Hydraulic Laboratory and its students. The test section where PIV and SPIV were conducted will be discussed in the following sections. Nolan Goth [10] performed multiple material studies for matching indices of refraction of solid and liquid materials that could be used for MIR PIV experimental facilities. The knowledge and studies provided by Goths research and advice made a lasting impact on the design of the primary facilities.

5.1 Materials Selection

Material selections for the experimental design loop were determined based on compatibility of indices of refraction, and chemical resistance for test section and fluid, and mechanical parts, respectively. Nolan Goth performed optical and mechanical testing on multiple solid/fluid pairs [10] determining that the use of p-Cymene and PMMA would be acceptable for MIR facilities used for PIV with indices of refraction of 1.491 and 1.49, respectively. Flexible hoses were used to connect the inlet and outlet of the test section to the pump and reservoir,

respectively. These hoses have to be chemical resistant material that was there for compatible with p-Cymene and were made from Ultra-High-Molecular-Weight Polyethylene (UHMWPE). The Final selection of the materials can be seen in Table 5.1.

Table 5.1: Material selection used for the experimental facility

	PMMA	SS316	Viton	UHMWPE	P-Cymene
Test Fluid					X
Test Sections	X				
Piping		X			
Pump		X	X		
Gaskets			X		
Flexible Hosing				X	
Reducer/Diffuser		X			
O-rings			X		
Reservoir		X			
Pebbles	X				

The experimental facility and the components will be discussed in the following sections. Figure 5.1 shows an example of the optical clarity achieved with a PMMA test section, pebbles, and p-Cymene fluid. Figure 5.1 gives an example of how the MIR fluid can create an optically clear environment between the pebbles and p-Cymene versus pebbles in air or a none MIR fluid.

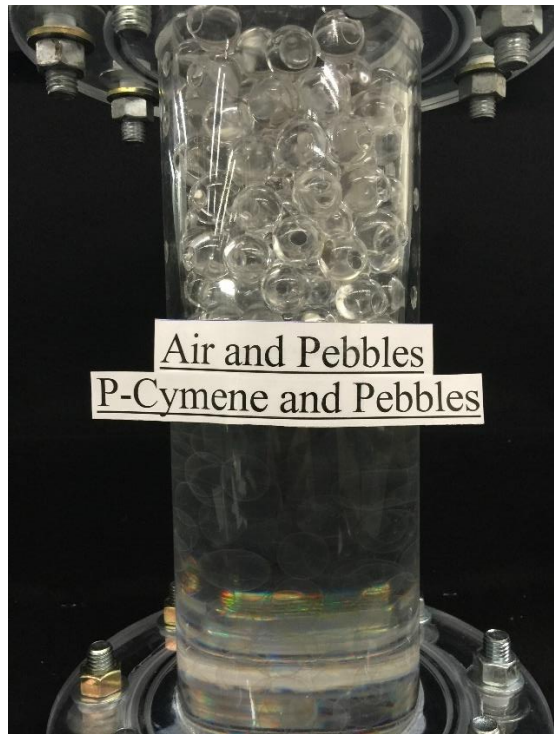


Figure 5.1: Small PMMA pipe filled with PMMA pebbles p-Cymene and air

The pebble bed facility was also designed with the ability to change the D/d_p aspect ratio between experiments. This was done to ensure that a wide variety of porosity oscillations could be achieved throughout the study. Pebble sizes were determined to range from 31.75-12.7mm in diameter with ratios ranging from 4.4-11. Figure 5.2 shows a scale of pebbles to be used during the two MIR experimental setups.



Figure 5.2: Scaled pebbles next to ruler ranging from 31.75 mm to 12.7 mm

5.2 Test Section

The MIR pebble bed test section included the following components:

5. Square inlet tube
6. Diffuser
7. Main inlet pipe
8. Hexagonal test section pipe
9. Main outlet pipe
10. Reducer
11. Rectangular upper plenum

All components but the diffuser and reducer are made of PMMA to ensure the index of refraction matching would be achieved for velocity measurements that would later be performed. The diffuser and reducer were both made of SS316 for corrosive resistance and contained perforated plates also made of SS316 to ensure pebbles would be isolated to the test section piping. The plates were made in house to hold the weight of the pebbles while also allowing the working fluid to circulate freely through the loop. Early testing found that the 0.5 horse-power (hp) pump

used for the pressure and MIR experiment could create a high-enough flowrate to cause the entire bed to shift. Therefore, the Variable Frequency Drive (VFD) was limited to a maximum of 45hz out of 60hz. This limitation ensured the test bed did not shift and the experimental interrogation area had no changes in geometry.

Each experimental facility contained only one loop. Testing done during the pressure-bed experiments found that the pump was not high enough power to cause any significant temperature change in the working fluid. The temperature shift in the liquid would cause the index of refraction to shift further from that of the solid.

5.2.1 Facility One

The primary coolant flows directly through a core of graphite spheres in PBRs. The flow through the bed is random and completely determined by the beds interstitial flow paths. Flow paths are also created randomly and dynamic because of the constant sorting. The pebbles flow down through the core hopper before being sorted and then put back into core circulation or removed. As seen in Figure 3.1 the oscillating porosity is a function of the sphere diameters from the wall of the core hopper to the center. This oscillation due to wall effects can create significant temperature differences in this region of bypass flows. PBRs can come in a High-temperature gas cooled reactor (HTGR) and MSR design that employs the use of 6 cm and 3 cm pebble diameters, respectively. The primary facility used ~ 3 cm diameter pebbles in a much smaller hopper section creating a D/d_p ratio of 4.4 which would ensure a large variation in porosity throughout the test section. Figure 5.3 shows (a) and isometric over view of the first MIR facility, (b) the first experimental facility test section constructed with the PMMA pebbles loaded inside, and (c) clean p-Cymene filling the hexagonal test section for reference of optical clarity.

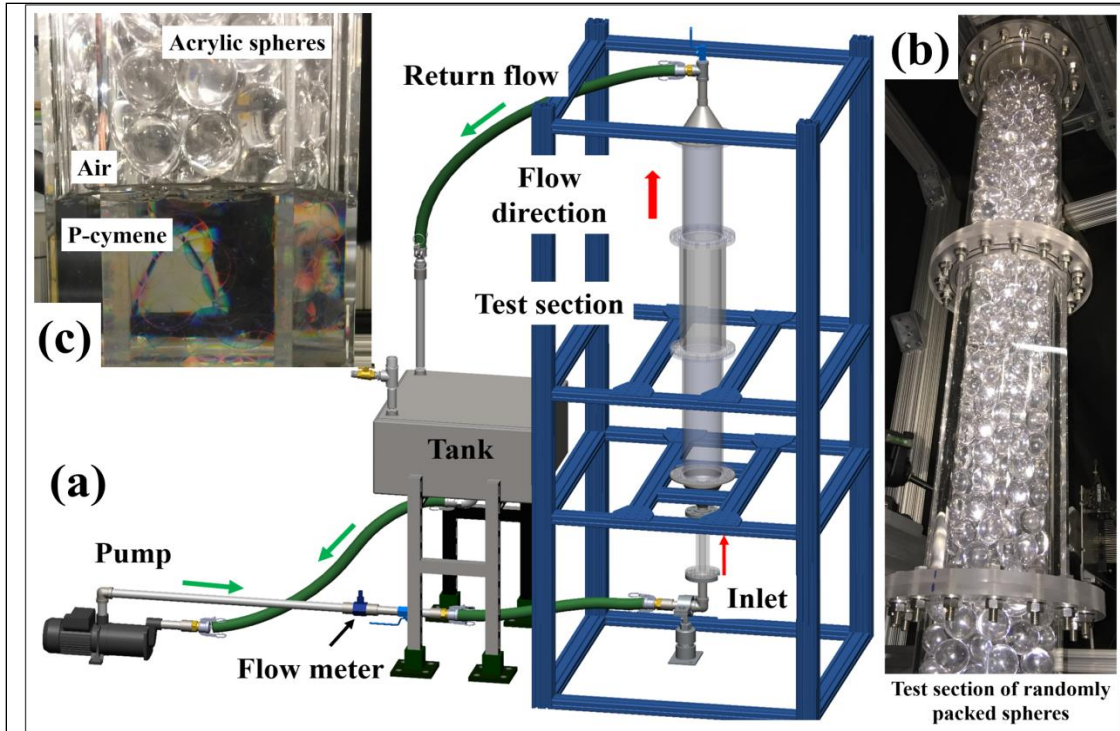


Figure 5.3: (a) Isometric over view of first facility, (b) facility filled with PMMA pebbles, and (c) photo of fresh p-Cymene filling test section

Figure 5.3 (a) shows in the isometric view with the listed parts the square inlet for inlet condition measurements, diffuser, main inlet pipe, hexagonal test section for PIV, main outlet pipe, and reducer. The list of measurements for these specific parts can be seen below in Table 5.2.

Table 5.2: Experimental test section one measurements

Parameter	Value (m)
Main Pipe Diameters	0.1397
Pebble Diameter	0.03175
Diffuser / Reducer Inlet and Outlet Diameters	0.0254, 0.1397
Main Pipe Heights - Inlet, Hexagonal, Outlet	0.508, 0.4572, 0.4064
Total Test Bed Height	~1.4
Square Inlet Pipe Height and Diameter	0.2413, 0.0254

The diffusers were fabricated by a company in Bryan, TX, Brazos Industries LLC. The main test section pipes as well as the square inlet pipe was fabricated by Moore Fabrication, a custom plastics fabrication shop in Houston, TX. All main pipes were formed from single pieces including the square inlet and hexagonal test section. Moore Fabrication specializes in creating unique geometries out of plastics this particular piece along with the square inlet section were created similarly. Rotating the pipe azimuthally around the axis by specified degrees and shearing sides to specific thicknesses. The exact measurements of all test section components can be found in Appendix A. Test section pipes were then polished until optically clear allowing for PIV techniques to be used for measurements through the walls while maintaining the circular inner pipe. The hexagonal test section, square inlet tube, and reducer can be seen below in Figure 5.4.

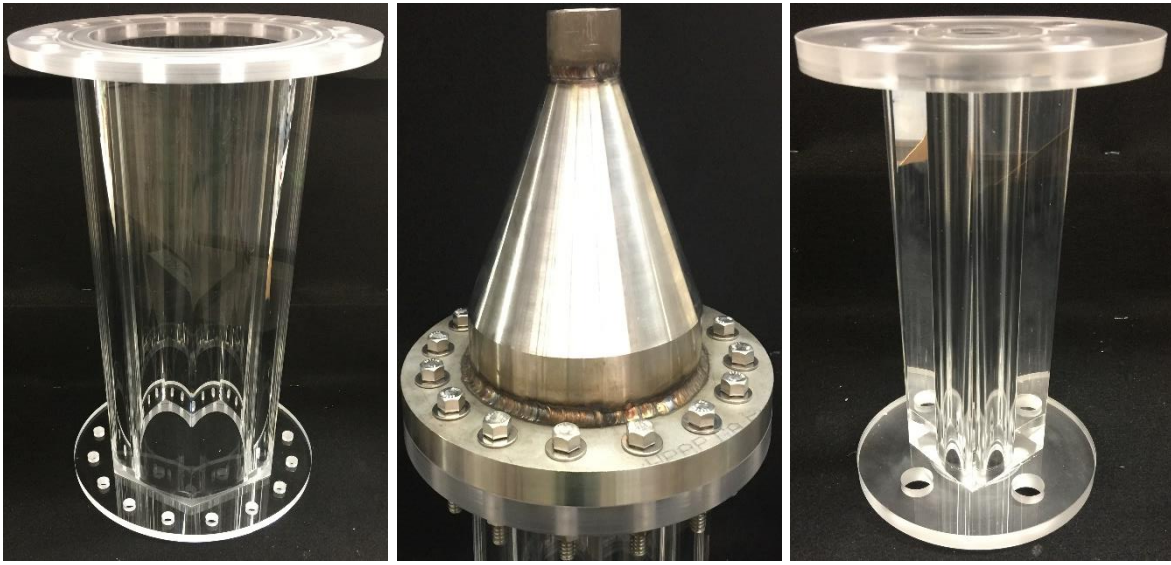


Figure 5.4: The hexagonal test section (left), reducer (middle), and square inlet pipe (right)

The fully assembled primary loop was made to circulate p-Cymene in the direction seen in Figure 5.3. The experimental facility was constructed and filled with pebbles and can be seen in Figure 5.5 with the square inlet tube featured to its right. The proof of concept achieved through the construction of the pressure facility allowed for the quick construction of the MIR facility. Through the use of the perforated steel plates installed inside the reducer's seclusion of the pebbles in the main test section was achieved while still allowing direct and even flow to enter the facility. The facility main test sections piping was connected completely by flanges. The upward facing flange on each pipe and the base diffuser was designed with two O-ring grooves in order to place Viton O-rings. These were created in to ensure a liquid tight seal during full flow.

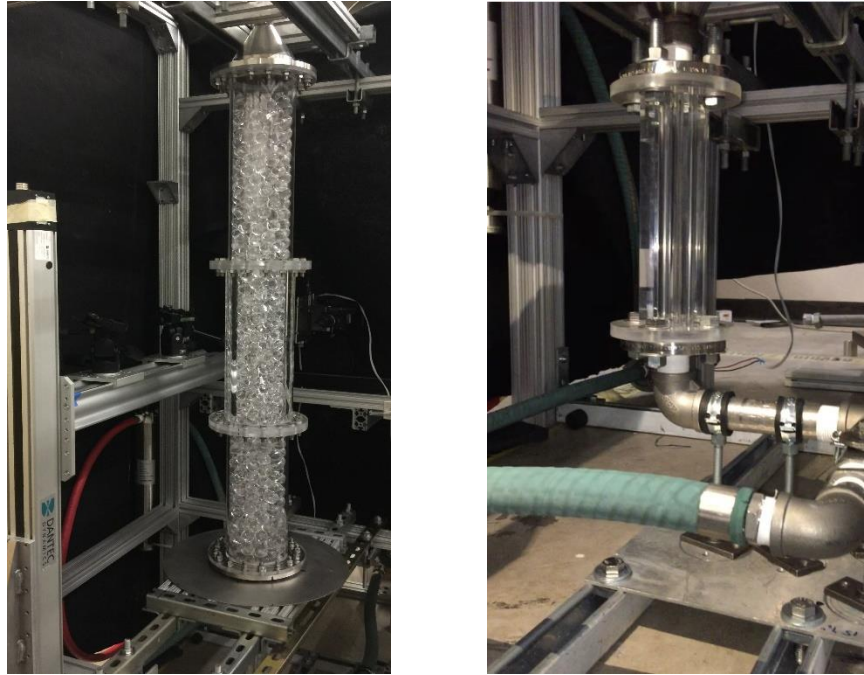


Figure 5.5: Experimental facility fully installed (left) with square inlet tube base (right)

Experimental facility one was constructed of three main pipes interconnected by flanges. This design was created in order to ease in the pebble replacement process and maximize test bed size. Supports can be seen in Figure 5.5 at the base of the square inlet pipe, main pipe inlet, and reducer outlet. The supports constructed were to reduce stress on the PMMA square pipe, hold the weight of the entire test section, and stabilize and properly orient the facility, respectively.

5.2.2 Facility Two

The second facility created during this experiment was introduced to allow for top down viewing of the test bed. The facility changes removed the main inlet and main outlet pipes, as well as the top reducer and added a rectangular upper plenum. The test section was reduced to the following components:

- Square inlet pipe

- Steel diffuser
- Hexagonal test section
- Upper plenum

The upper plenum, a rectangular PMMA box, was connected by pipe and flange to the hexagonal test section and had two outlets. The outlets were created at opposite corners to enable symmetric out flow of the fluid as well as an obstruction free interrogation area directly over the test bed. This final piece was constructed after determining radial measurements were needed to complete the first objective listed. A 3D Computer-aided Design (CAD) representation of the second facility can be seen in Figure 5.6. This CAD design also shows the flow direction as well as the PIV setup to be used for radial flow measurements.

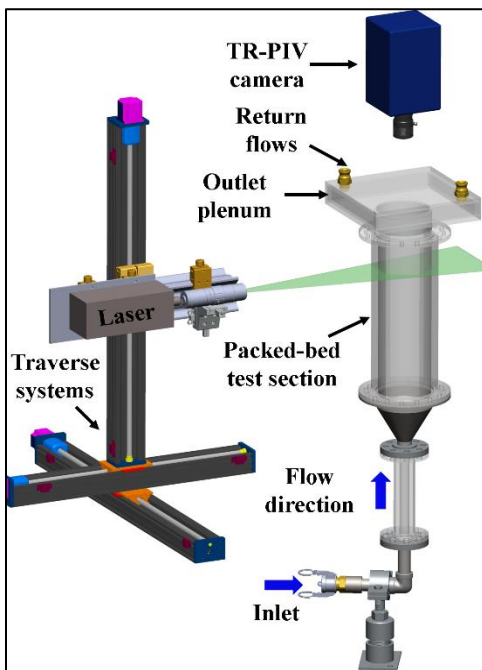


Figure 5.6: Cad of experimental setup two



Figure 5.7: Experimental facility two

The assembled experimental facility with the upper plenum addition can be seen in Figure 5.7. The spheres placed inside the final experimental setup were 2.2225 cm (7/8 in) in diameter giving a D/d_h of 6.28. The primary loops of both experimental setups contained roughly the same main components and followed the same flow directions. Hosing supports were installed on the second facility in order to reduce mechanical stress and vibrations on outlet ports of the upper plenum.

The main flow components of both the experimental loops are provided below:

- 0.5 hp (horse power) pump
- Variable Frequency Drive (VFD)
- Inline Blanchette 1100 turbine flow meter
- Reservoir tank 25-gallon
- 1-inch UHMWPE flexible chemical hoses
- 1-inch SS316 diameter piping and valves
- Test section
- Silver seeding particle injection port
- Upper plenum

5.3 Leak Testing

The first and second experimental test loops were both tested for leaks the same way. The loops were first assembled completely without pebbles and filled fully with p-Cymene. The maximum flow rate, $3.41 \text{ m}^3\text{s}^{-1}$ (15 gallons-per-minute (GPM)), was assumed to be low enough that leakage from section connections would not be a prominent problem. The double O-ring flanges and pipe connections showed no leaks during full flow of the leak tests or operation.

Threaded pipe connections were all sealed with Polytetrafluoroethylene (PTFE), Teflon™, and all flange seals consisted of chemically resistant Viton O-rings.

5.4 Imaging hardware

This section consists of descriptions of the PIV setup for the first and second experimental facility designs. The hardware specifications will also be found in this section with details about the PIV process followed.

5.4.1 PIV Setup and Hardware

Fig. 5.8 (a) shows the experimental configuration of the two-dimensional two-component (2D2C) TR-PIV measurements in the facility of randomly packed spheres, while Fig. 5.8 (b) illustrates a cross-section of the visualization section. The visualization systems of PIV consist of a high energy laser allowing pulse rates of up to 20 kHz, coupled with high-speed CMOS cameras that are capable of frame rates up to 3.2 kHz at full 1280 x 800 resolution with up to 14-bit sensitivity and shutter speeds as fast as 2 μ s. A laser light sheet will be formed and directed to illuminate the experimental test section utilizing high-energy mirrors and beam shaping optics. Macro-zoom lenses will be used to obtain high-resolution images of the internal flow field within milli- to micro-second time intervals, thereby enabling the use of advanced ensemble correlations to provide flow field measurements.

The TR-PIV system consisted of a 20 W continuous laser with a wavelength of 527 nm and two high-speed CMOS Phantom M310 cameras. The laser head was mounted on linear traverses, and the laser beam was adjusted by using a combination laser optics (TSI 610026) to create a 1-mm-thick laser sheet. The Phantom M310 cameras had a pixel size of 20 x 20 μ m, a 12-bit depth image of 1280 x 1280 pixels at its full resolution, and an internal 12 GB memory.

The high-speed cameras were attached with Zeiss 105-mm camera lenses, $f/5:6$ apertures, and mounted on three-axis motorized linear translation stages. For the PIV measurements, seeding particles were hollow glass spheres with a mean diameter of $10\ \mu\text{m}$. The particles were pre-mixed in the tank, driven by the pump, and re-circulated through the entire flow loop to ensure their presence throughout the entire test section and a homogeneous mixture was achieved.

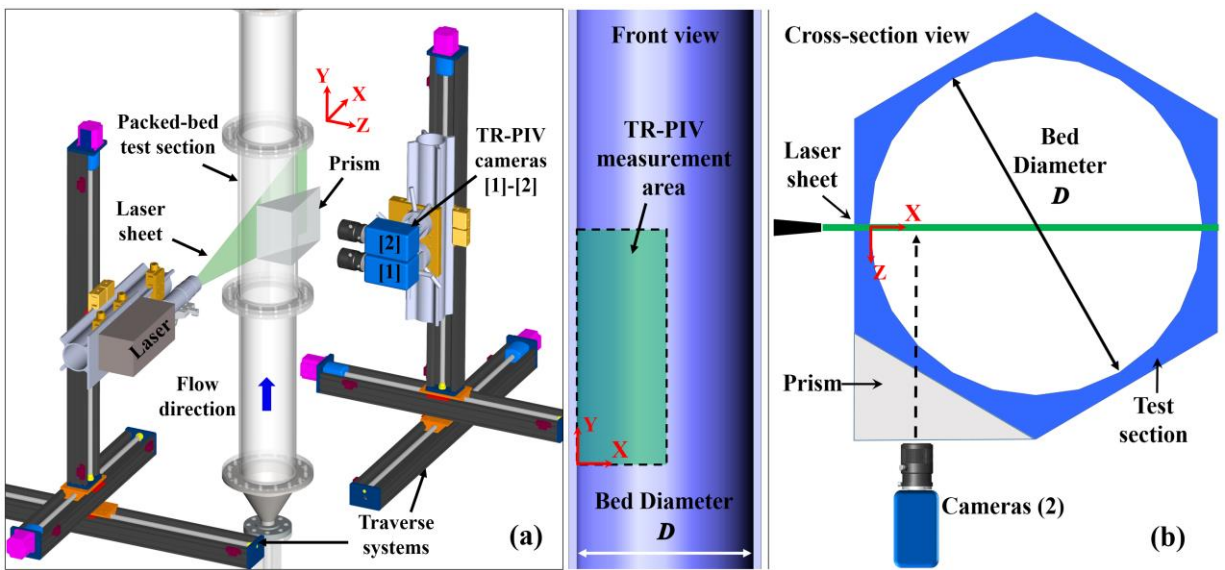


Figure 5.8: (a) Experimental setup of time-resolved PIV measurements, (b) front-view and cross section of the visualization section

Figure 5.9 shows the experimental set up filled with air, p-Cymene, and during laser operation. The operational set up with optical prisms to correct the angle against the hexagonal test section and square inlet section can be seen in Figure 5.10.

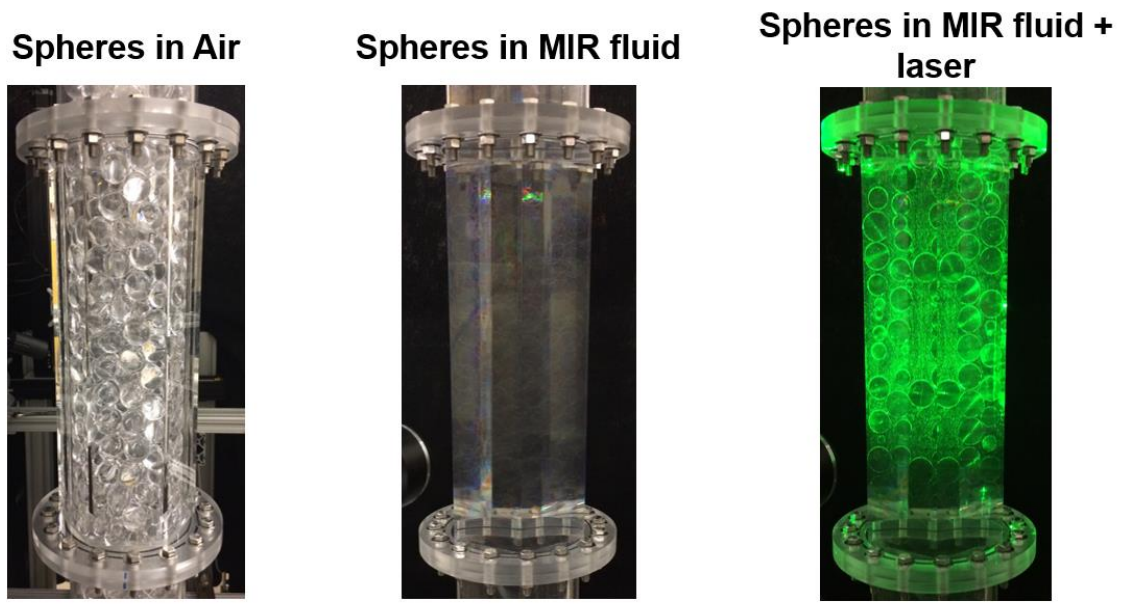


Figure 5.9: Experimental test section during filled with air (left), p-Cymene (middle), and during operation (right)

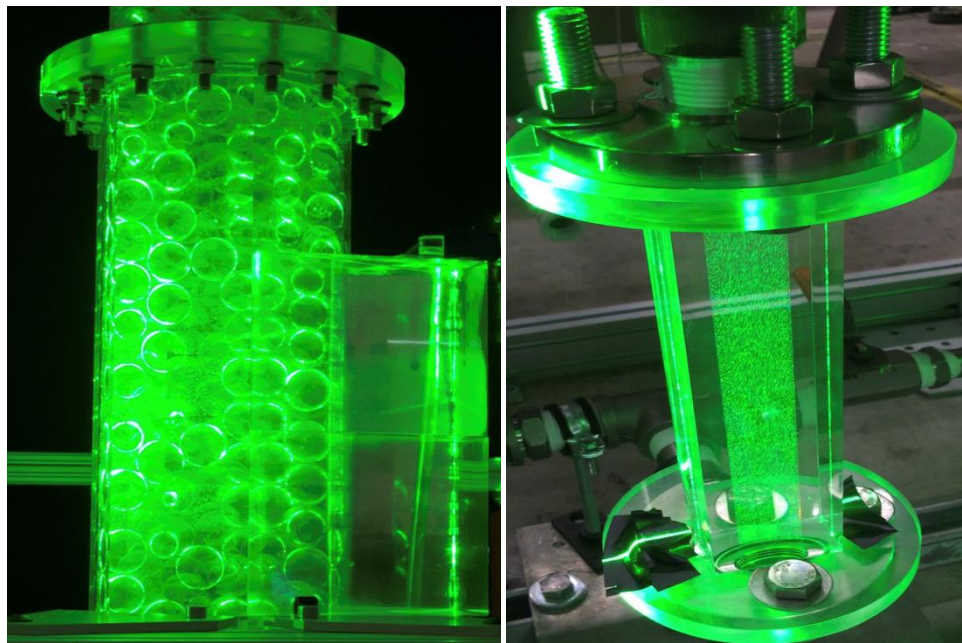


Figure 5.10: Hexagonal (left) and square (right) sections during operation

The vertical plane created was located at the center of the visualization section with images taken on near the pipe wall. A 30-60-90 triangular prism was used to create a visual for the cameras that would be perpendicular to the laser plane created. This triangular prism was attached directly to the outside of the hexagonal test section. PIV was also performed on the square inlet test section in order to perform inlet condition characterization and flow rate verification.

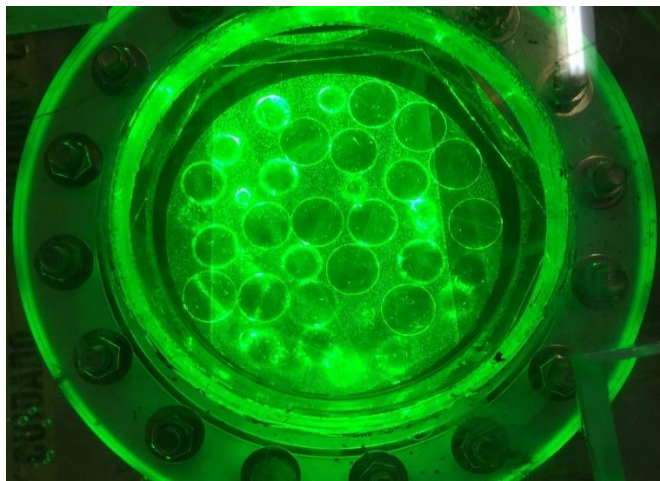


Figure 5.11:Top down radial PIV through upper plenum of second facility

PIV was also conducted on the second facility in the vertical direction in the same way as the first facility design. However, the addition of the PMMA plenum allowed for downward viewing to gather radial velocity measurements as well as scan the pebble bed and can be seen in Figure 5.11.

6 FACILITY TWO TEST BED SCAN

The PMMA plenum was originally built in order to perform radial velocity measurements. Vertical measurements were first performed using the same method seen in Figure 5.9 on the first facility. The top three inches of the hexagonal test-section were measured in order to reduce the number of sphere diameters being viewed through during top-down radial measurements. Due to the time needed to process data, results for vertical and radial PIV are not presented. However, a 3D CAD test bed reconstruction was able to be completed. Using a view perpendicular to the horizontal laser sheet and radius of the hexagonal pipe from the top of the facility a scan was performed. The laser, camera, and facility setup as well as one of the images taken during the scanning process can be seen in Figure 6.1 below.

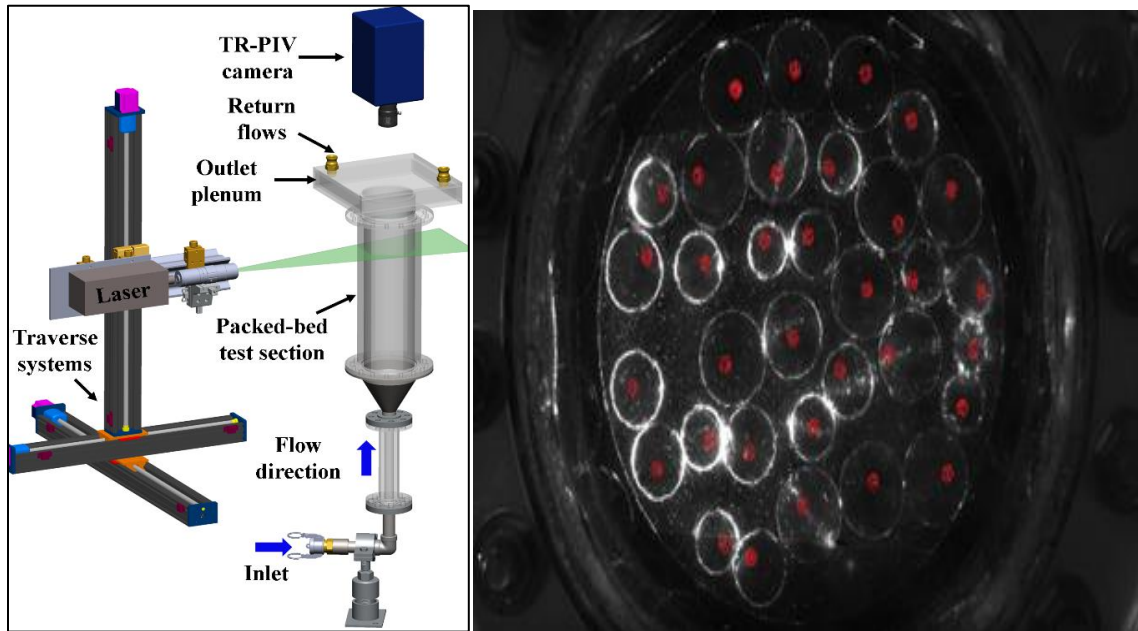


Figure 6.1: Test bed scan setup (left) with actual test bed scan image (right)

The laser was positioned -8.89 cm (3.5 in) below the top flange with the camera positioned high enough over head to observed the entire cross section of the pipe. The camera and laser were both mounted to 3D traversal systems and simultaneously moved upward axially by 0.3175 cm (0.125 in) after each image was taken until the laser was -1.27 cm (0.5 in) below the top flange. A total of 25 consecutive images were taken over the span of 7.62 cm (3 in) each containing the entire cross section of the pipe. Using a 3-point circle recognition macro created for ImageJ software the x and y pixel centroid and pixel radius of each individual sphere and pipe cross-section was determined.

A total of 148 spheres were counted within the scanned section. The XY origin was located at the top left corner of each image creating a 13.97 x 13.97 cm (5.5 x 5.5 in) square with the x and y axis tangent to the pipe's top and left side, respectively. The conversion process from pixel to a measured distance relied on knowing the inner diameter of the pipe cross-section. Using the pixel conversion for each individual picture the XY locations and height difference was calculated. The consecutive images helped to determine when a new pebbled entered the image as well as whether the cross-section of the pebble being measured was from above or below its true centroid. Thus, the equation became:

$$h = \sqrt{R^2 - r_c^2} \quad \text{Eq. 2}$$

Where h is the height difference of the cross-sectional scan to the z centroid, R is the radius of the pebble and r_c is the radius of the pebble's cross-section at the laser scan known height. Knowing whether this cross-sectional scan was on the top or bottom of the pebble made the determination

of the centroids z location a simple addition or subtraction from the laser's actual height. The miss calculation of 4 out of the 148 spheres was determined after a primary 3D CAD replica was created by generating spheres around the centroids, and then cross-referencing the CAD cross-section images with actual experimental images. One of the image pairs taken of the 3D CAD and PIV cross-sections can be seen in Figure 6.2.

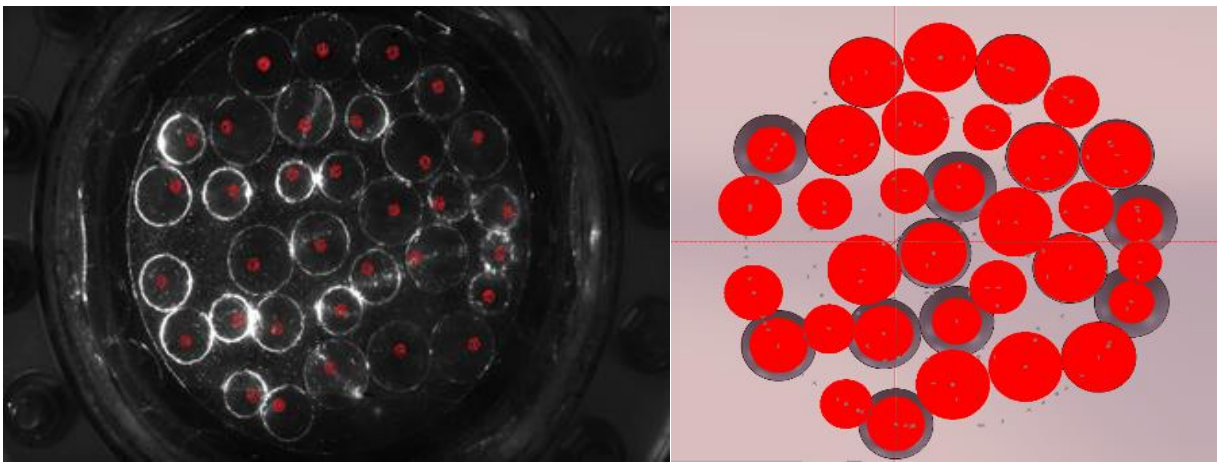


Figure 6.2: Image pair used to verify reconstruction accuracy

The reconstruction was verified by comparing the PIV images with the corresponding CAD cross-section images. This comparison process was used to find the final four sphere miscalculations. The final list of centroid locations calculated can be found in Appendix B, with all image pairs found in Appendix C. The final 3D CAD reconstruction image can be seen below in Figure 6.3.

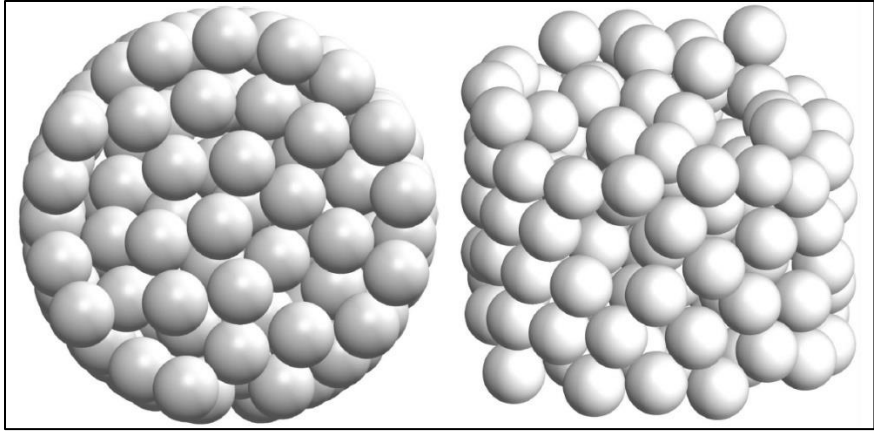


Figure 6.3: 3D CAD experimental pebble bed reconstruction

7 PARTICLE IMAGING VELOCIMETRY

In order to meet the requirements of the first objective of performing non-intrusive flow measurements PIV was employed. This is an optical measurement technique performed to quantify displacement of particles within a flow assuming the particles follow the flow perfectly.

To measure the velocity and displacement of the flow without intrusive instrumentation the use of reflective seeding particles is employed. The seeding particles used were silver-coated hollow glass spheres with a mean diameter of 16 μm , yielding a good particle image intensity. The particles were re-mixed in the primary tank before being circulated through the entire flow loop. The particles must be thoroughly mixed and present throughout the test bed to ensure an adequate amount of reflected light and high enough density that an accurate flow representation can be achieved. These particle groupings reflect light while traversing the laser sheet in the interrogation window and are captured by a CCD/CMOS digital camera to create an image. The displacement of the particles is then cross-correlated between consecutive images. Nolan Goth gives an in-depth description here [10] of the methodology of PIV and won't be discussed in this thesis.

Figure 5.7 (a) shows how the horizontal cross-sectional measurements were achieved on the pebble bed facility. The vertical laser sheet was used to illuminate the left half of the facility as the cameras viewed through the triangular prisms. The camera interrogation windows were made to slightly overlap one another and triggered simultaneously in order to create a continuous PIV image. The coordinate system created for the horizontal and vertical directions in the window was done through the calibration images.

Three dimensional traverses were used on both the laser and cameras allowing for control as the bed was scanned in the Z direction. Creating a calibration image was done knowing the diameter of the sphere being measured. By monitoring of the cross-section of a single sphere the

laser sheet was moved known distances until the cross-section of the sphere had reached a maximum size. The camera was then moved approximately the same distance in the z axis to capture an image that would be used. Measuring the diameter of the spheres cross section was done to determine pixel to distance conversions for the consecutive images taken during experimental operation. Figure 7.1 shows examples of the raw PIV images taken during operation.

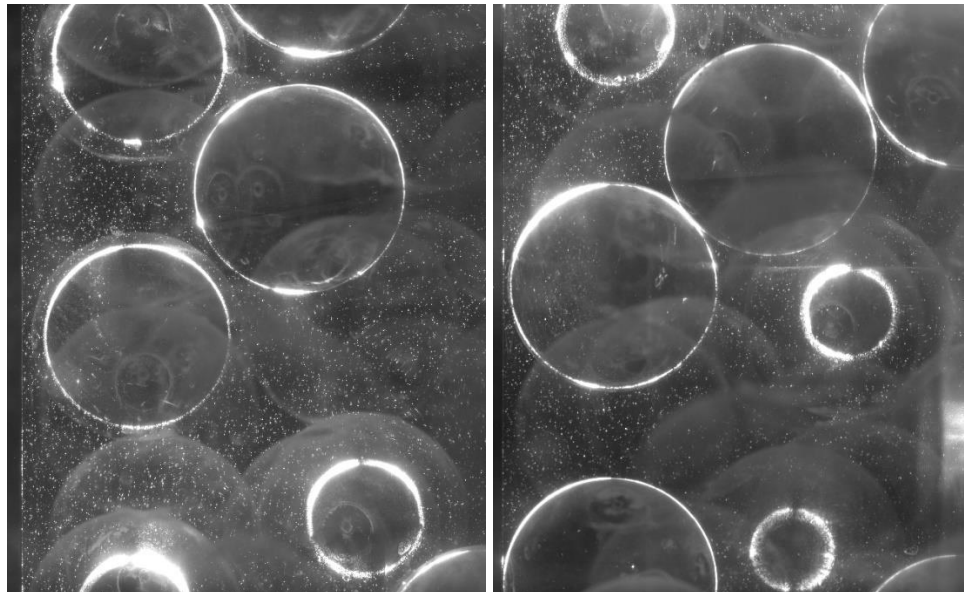


Figure 7.1: Raw PIV images from top (left) and bottom (right) cameras during operation

The cameras images contained some overlap in order to create a single interrogation window. The example can be reconstructed using the images seen above in Figure 7.1. The combination of these structures can be seen in Figure 7.2 with each image outlined. This additional overlap and simultaneous camera triggering created a continuous uninterrupted PIV image. For each studied Reynolds number, three experimental runs were performed. For each experimental

run, the cameras captured a sequence of 16681 images of 640×800 pixels in a single-frame mode with frequencies ranging from 200 fps to 800 fps corresponding to the Reynolds numbers ranging from 340 to 720. The experimental runs were done three times for each Reynolds number in order to compute the flow statistics.

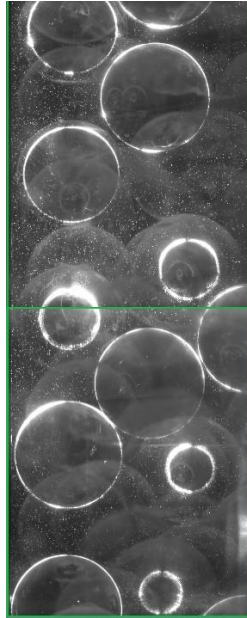


Figure 7.2: Combined images from top and bottom cameras

All PIV images captured by two cameras were processed by the advanced multi-pass, multi-grid PIV processing algorithms implemented in the PRANA codes [11]. In the PIV processing, the initial and final interrogation windows were 64×64 pixels and 32×32 pixels, respectively. Initial and final passes had a 50% and 75% window overlap, respectively, and yielded a final spatial gap between two adjacent vectors of 0.89-mm. Velocity vectors were calculated from the correlation map with a Gaussian peak fit for sub-pixel accuracy [12]. A median filter [13] was applied, standard deviations of the neighboring vectors were used to filter out spurious vectors, and then

blanks were filled by velocity interpolation. Velocity vector fields obtained from two cameras were adjoined and interpolated to yield the larger field of 198×77 vectors.

8 PIV RESULTS

Statistical results obtained from experimental measurements in the packed spheres by using TR-PIV technique are presented in previously published article by E. Kappes et al with permission from ASME [14,15]. Collections of velocity vector fields corresponding to three experimental runs for each Reynolds number are used to compute the flow statistics, such as mean velocity, root-mean-square (rms) fluctuating velocity, and Reynolds stress component.

These are some of the experimental results obtained from the TR-PIV measurements at the vertical plane corresponding to three Reynolds numbers $Re_1 = 340$, $Re_2 = 520$, and $Re_3 = 740$ are shown in Figure 8.1. The top row shows the instantaneous results, while the bottom row illustrates the time-averaged results. The PIV velocity vectors and contours were plotted over masks created from bed images to aid the visualization of the internal flows within the packed spheres. It can be seen from the instantaneous velocity vector fields in Figure 8.1 that when the Reynolds numbers increased, the flow turbulence and flow mixing also increased. The mean velocity vector fields and magnitudes computed from three Reynolds numbers, however, revealed approximately similar flow patterns. The stagnation and recirculation zones become more localized and defined as the velocity of the flow is increased creating well defined regions within the flow patterns. As the spheres inside the facility were randomly packed, spatial gaps between neighboring spheres were randomly distributed over the entire volume of the test section. In the current PIV field of view, the spatial gaps varied from ~ 4 mm to ~ 35 mm, approximately from $0.12dp$ to $1.1dp$. Such variations of local spatial gaps defined the instantaneous flow patterns within those regions. For example, the local flow structure, such as the circulation zone, of the sphere's section located at $(x,y) = (46,40)$ mm had smaller size compared to those of the sphere's section located at $(x,y) = (15,85)$ mm and $(x,y) = (44,98)$ mm.

Figure 8.2 illustrates the mean velocity vector fields overlaid on the color contour of out-of-plane vorticity magnitude. These plots confirmed similar overall flow trends within the packed spheres despite an increase in Reynolds. These figures show the positive and negative shear layers created by interactions between the axial flow flowing upward and the trailing edge of the spheres. It can be seen that as the Reynolds numbers increased, magnitudes of the mean velocity and vorticity also increased at the same order. Figure 8.2 consists of measurements in the facility of randomly packed spheres for the Reynolds numbers of $Re_1 = 340$ (left), $Re_2 = 520$ (middle), and $Re_3 = 720$ (right). (Top row) Instantaneous velocity vector, color contour of velocity magnitude (m/s). (Bottom row) Time-averaged velocity vector and color contour of velocity magnitude (m/s).

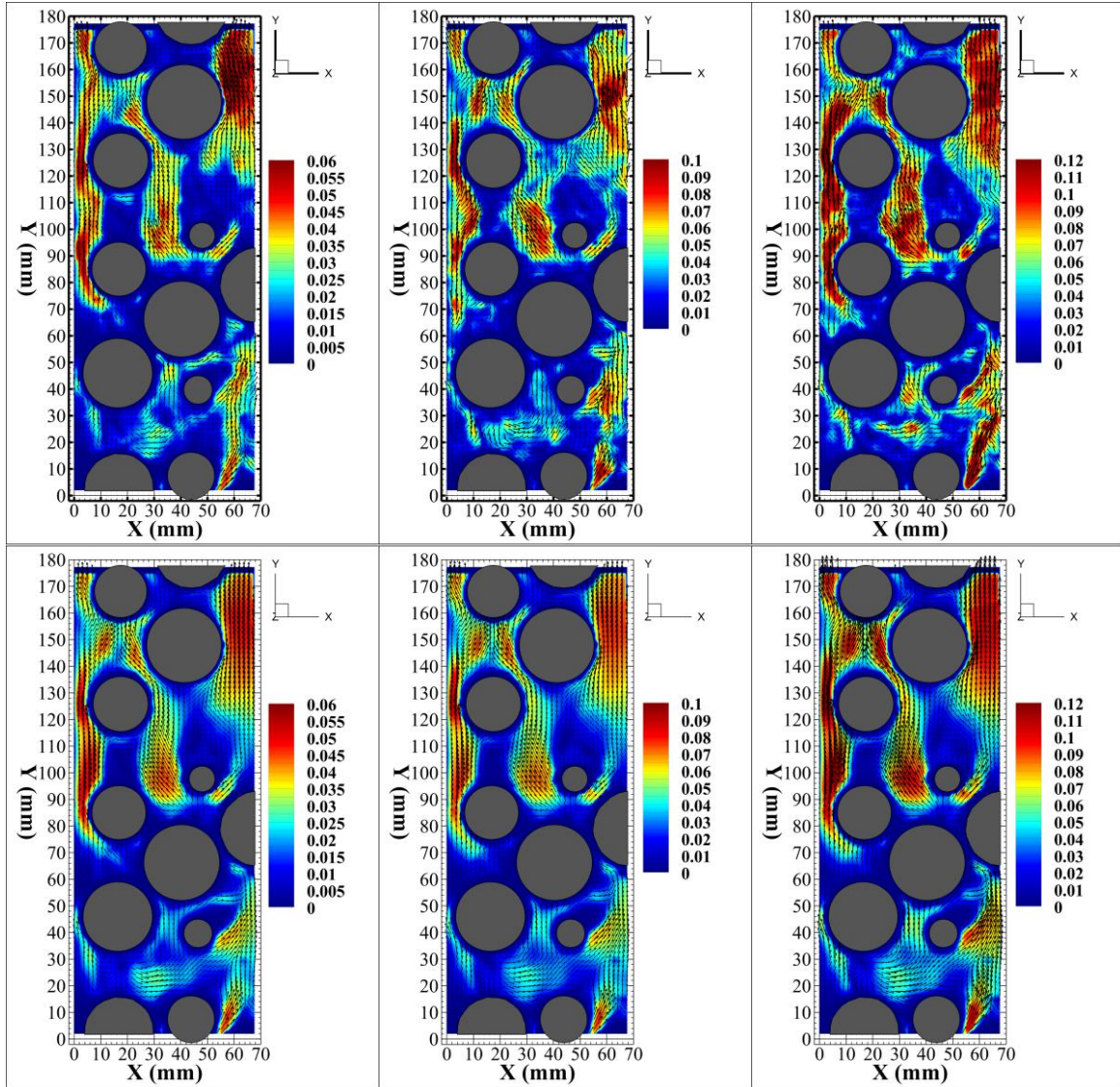


Figure 8.1: Velocity vector and color contour of velocity magnitude TR-PIV results [14] reprinted with permission Copyright © 2018 by ASME

Figure 8.2 shows the time-averaged velocity vector and color contour of z -vorticity (1/s) results obtained in the facility of randomly packed spheres for the Reynolds numbers of $Re_1 = 340$ (left), $Re_2 = 520$ (middle), and $Re_3 = 720$ (right).

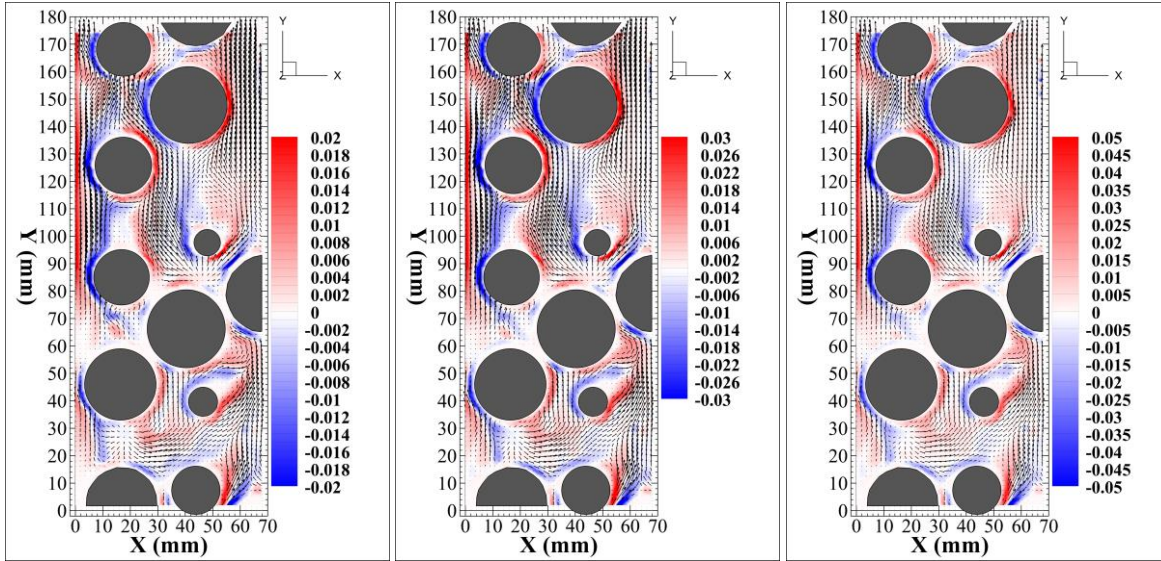


Figure 8.2: Velocity vector and color contour of z-vorticity results from TR-PIV measurements [14] reprinted with permission Copyright © 2018 by ASME

Vorticity magnitude seems to be less sensitive as the Reynolds numbers increased with the recirculation and stagnation zones remaining approximately the same size only to be more defined at their edges. When the axial flow is directed and impinges on the upstream side of spheres, it was forced to divide into smaller by-pass flows. This divide creates the opposite vorticity fields located on the sides of the medium and large sphere cross-sections. Moreover, as the spheres are randomly packed into the three-dimensional volume of the test section, after impinging into the spheres' upstream sides, the by-pass flows could follow multiple directions in associated with locations of neighboring spheres. Depending on the random locations of the spheres and the mass flow rates of branch flows, the flow impingement may create strong shear layers and recirculation regions downstream of the spheres. These above phenomena can be observed in the complicated flow patterns revealed by the instantaneous and mean velocity fields, and mean vorticity fields.

In Figure 8.3, color contours of root-mean-square (RMS) fluctuating horizontal and vertical velocity components, i.e. $\sqrt{\overline{u'^2}}$ and $\sqrt{\overline{v'^2}}$, and Reynolds stress $\overline{u'v'}$ computed from TR-PIV measurements at the Reynolds number of $Re_3 = 720$ are displayed. It can be observed from figure 6 that $\sqrt{\overline{u'^2}}$ and $\sqrt{\overline{v'^2}}$ contours showed the same maximum magnitude indicating the same order of flow turbulence for both horizontal and vertical velocity components. Color contour of the Reynolds stress reached the maximum downstream and both side of the spheres. Such high Reynolds stress values were generated by the shear layers when the axial flow passed the spheres and detached from the upstream side. Figure 8.3 shows results from the facility of randomly packed spheres for the Reynolds number of $Re_3 = 720$. (Left) Root-mean-square fluctuating horizontal velocity $\sqrt{\overline{(u'^2)}}$ (m/s), (middle) root-mean-square fluctuating vertical velocity $\sqrt{\overline{(v'^2)}}$ (m/s), (right) Reynolds stress $\overline{(u'v')}$ (m²/s²).

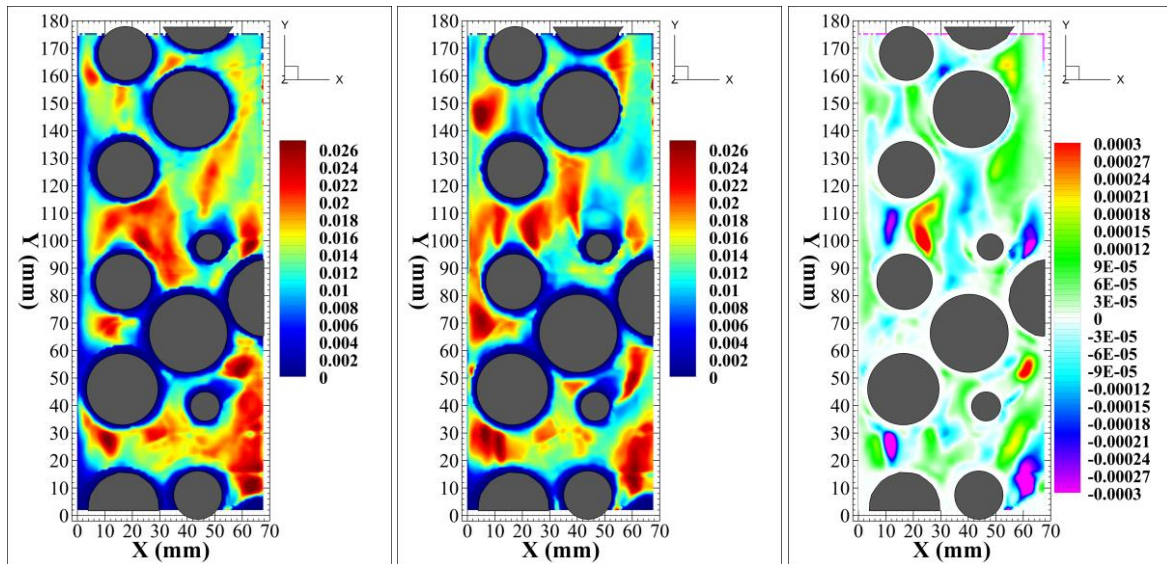


Figure 8.3: RMS results of fluctuating horizontal velocity (left), vertical velocity (middle), and Reynolds stress (right) from TR-PIV measurements [14] reprinted with permission Copyright © 2018 by ASME

The first- and second-order statistical results, such as mean velocity, rms fluctuating velocity, and Reynolds stress, computed from the TR-PIV measurements in the MIR facility of packed spheres at Reynolds numbers of $Re_1 = 340$, $Re_2 = 520$, and $Re_3 = 720$ are compared here. Statistical results were interpolated along the horizontal line 1 ($y = 105$ mm). The mean horizontal, U , and vertical, V , velocities, and rms fluctuating velocities, $\sqrt{u'^2}$ and $\sqrt{v'^2}$, were normalized by the mean velocity U_m , while the Reynolds stress $\overline{u'v'}$ was normalized by U_m^2 .

Figure 8.4 illustrates the comparisons of the normalized mean velocities, rms fluctuating velocities and Reynolds stress with various values of Reynolds. The flow statistics and velocity profiles at the axial locations within Figure 8.1 can be correlated to the locations within the snapshots of the pebble bed of Figure 8.3. It can be seen that with the increases in Reynolds numbers, both normalized velocities U and V maintain the same trend with exaggerated peaks. The increase of flow rates also yielded an overall augmentation in the magnitudes of the rms fluctuating velocities and Reynolds stress. In Figure 8.4(a), the mean horizontal velocity had its magnitude and sign changed when passing through the recirculation region downstream of the sphere. The rms fluctuating velocity profiles showed local maximal peaks whose horizontal locations were along the shear layers generated downstream of the spheres. Comparison of Reynolds stress $\overline{u'v'}$ profiles also showed similar trends with local positive and negative peaks appeared along the shear layers.

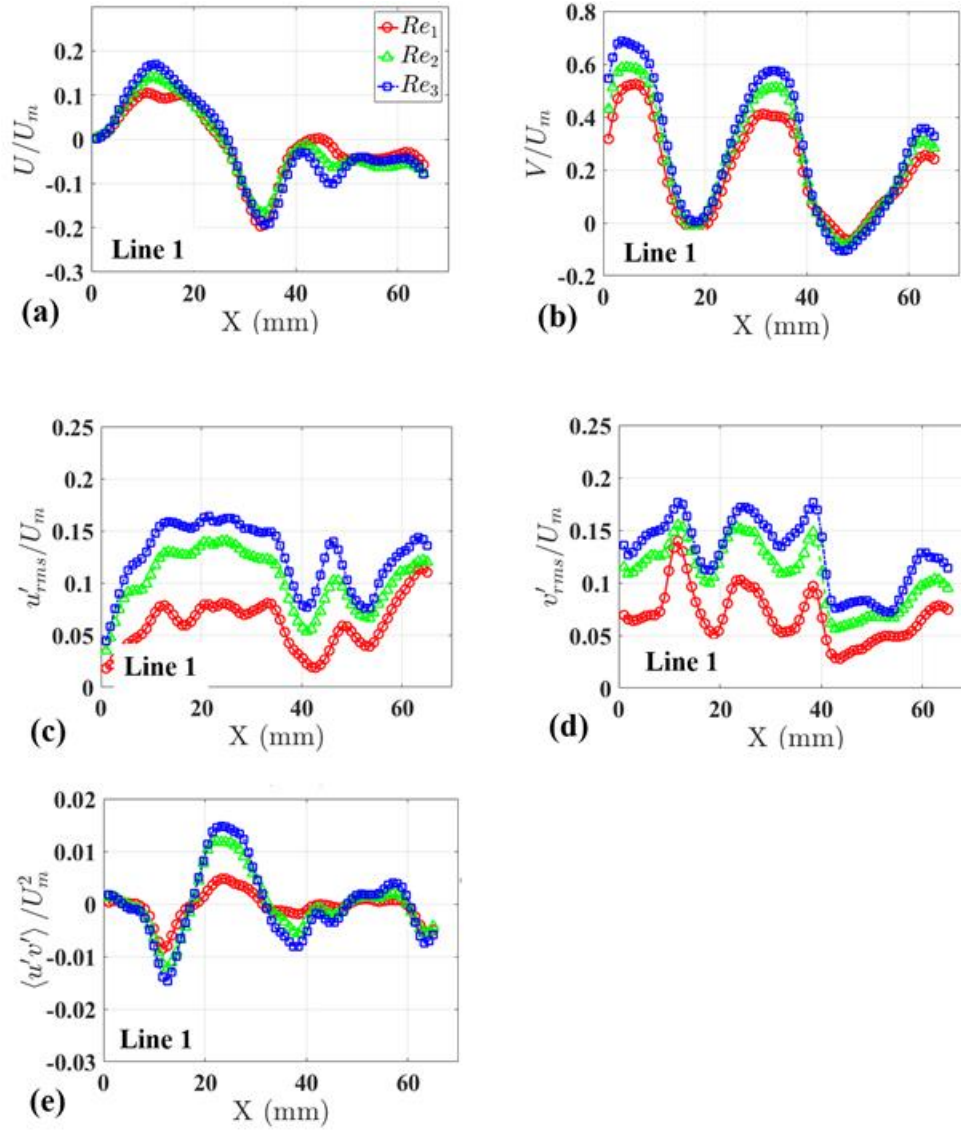


Figure 8.4: Comparison of statistical results obtained by TR-PIV measurements on the MIR facility of packed spheres for $Re_1 = 340$ (red), $Re_2 = 520$ (green), and $Re_3 = 720$ (blue) [14] reprinted with permission Copyright © 2018 by ASME

Results in Figure 8.4 were interpolated to Line 1 ($y = 105$ mm). (a) Normalized mean horizontal velocity U/U_m , (b) normalized mean vertical velocity V/U_m , (c) normalized rms fluctuating

horizontal velocity $\sqrt{(\overline{u'^2})}/U_m$, (d) normalized fluctuating vertical velocity $\sqrt{(\overline{v'^2})}/U_m$,
(e) Reynolds stress component $(\overline{u'v'})/U_m^2$.

9 CONCLUSION AND LESSONS LEARNED

This thesis has presented the design, construction and operation of the MIR pebble bed facility developed at TAMU's Thermal-Hydraulic Laboratory. Results from TR-PIV measurements in the MIR facility of randomly packed spheres that can be found in many engineering applications. Spatiotemporal resolved velocity measurements were performed along the central vertical plane of the experimental facility. The vector fields obtained from the TR-PIV measurements were used to calculate flow statistics, such as mean velocity, rms fluctuating velocity and Reynolds stress, for three Reynolds numbers, $Re_1 = 340$, $Re_2 = 520$, and $Re_3 = 720$. It was found that the overall flow patterns within the spatial gaps between spheres were created even at the low Reynolds numbers, and their sizes were not strongly influenced by the increase in Reynolds number. However, the flow turbulence and instantaneous flow patterns showed differences when Reynolds numbers increased. Complex flow structures were observed within the internal flows of packed bed, such as the presence of bypass flows created by the impingement on flow upstream and spheres, or the creation of recirculation zones and shear layers downstream of spheres. Statistical analyses of the TR-PIV results showed an increase in peak magnitudes but the overall trend of the flow patterns remained similar. The statistical analysis can be correlated precisely with the PIV snapshot results.

Future work will involve the use of the results obtained during TR-PIV both horizontally and radially from MIR facility two. The reconstruction of the test bed from the second MIR facility allows for a myriad of opportunities. When results lying within perpendicularly intersecting planes are fully analyzed and overlaid within the CAD reconstruction geometric effects and flow regimes will be understood far better than previously thought. The of a realistic 3D CAD reconstruction and overlaid results will be used for future verification and validation of CFD simulations of randomly packed structures.

REFERENCES

1. S.S. Penner, R. Seiser, K.R. Schultz, Steps toward passively safe, proliferation-resistant nuclear power, *Progress in Energy and Combustion Science*, Volume 34, Issue 3, 2008, Pages 275-287, ISSN 0360-1285, <https://doi.org/10.1016/j.pecs.2007.07.003>.
2. J. K. ARTHUR, D. W. RUTH, and M. F. TACHIE, "PIV measurements of flow through a model porous medium with varying boundary conditions," **Journal of Fluid Mechanics**, 629, 343–374 (2009).
3. S. KHAYAMYAN and T. S. LUNDSTRÖM, "Interaction between the flow in two nearby pores within a porous material during transitional and turbulent flow," **Journal of Applied Fluid Mechanics**, 8, 2, 281–290 (2015).
4. Y. A. HASSAN and C. KANG, "Pressure drop in a pebble bed reactor under high Reynolds number," **Nuclear Technology**, 180, 2, 159–173 (2012).
5. V. A. PATIL and J. A. LIBURDY, "Turbulent flow characteristics in a randomly packed porous bed based on particle image velocimetry measurements," **Physics of Fluids**, 25, 4, 043304 (2013).
6. King, E. Kappes, M. Marciniak, D.T. Nguyen, Y.A. Hassan, V. Ugaz,, "Pressure drop measurements in a versatile experimental facility of packed spheres", ANS Winter Meeting, 2017.
7. Hassan YA, Dominguez-Ontiveros E (2008) Flow visualization in a pebble bed reactor experiment using PIV and refractive index matching techniques. *Nuclear Engineering and Design* 238(11):3080–3085
8. Abdulmohsin, Rahman, "Gas dynamics and heat transfer in a packed pebble-bed reactor for the 4th generation nuclear energy" (2013). Doctoral Dissertations. 2178. http://scholarsmine.mst.edu/doctoral_dissertations/2178
9. Benjamin, Nelson L., "Scaling analysis for the pebble bed of the very high temperature gas-cooled reactor thermal hydraulic test facility" 2009. 2017-08-08. Master's Thesis.
10. Goth, Nolan Edward (2017). Design and PIV Measurements on a Wire-Wrapped 61-Rod Hexagonal Fuel Assembly Experimental Facility. Master's thesis, Texas A&M University.
11. A. Eckstein and P. Vlachos, "Assessment of advanced windowing techniques for digital particle image velocimetry (dpiv)," *Meas. Sci. Technol.*, vol. 20, 2009.
12. Raffel, M., Willert, C. E., Wereley, S. and Kompenhans, J., "Particle image velocimetry: a practical guide", Springer, 2013.

13. Westerweel, J., “Efficient detection of spurious vectors in particle image velocimetry data”, *Experiments in Fluids* 16(3-4), 1994, pp: 236–247.
14. E. KAPPES, M. MARCINIAK, A. MILLS, R. MUYSHONDT, S. KING, T. NGUYEN, Y. HASSAN, and V. UGAZ, “Time-Resolved Velocity Measurements in a Matched Refractive Index Facility of Randomly Packed Spheres”, *Proceedings of the 18th International Conference on Nuclear Engineering (ICONE26)*, London, England, (2018).
15. T NGUYEN, E KAPPES, S KING, Y HASSAN, V UGAZ, “Time-resolved PIV measurements in a lowaspect ratio facility of randomly packed spheres and flow analysis using modal decomposition”, *Experiments in Fluids* 59 (8), 127.

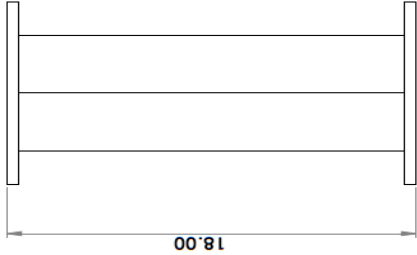
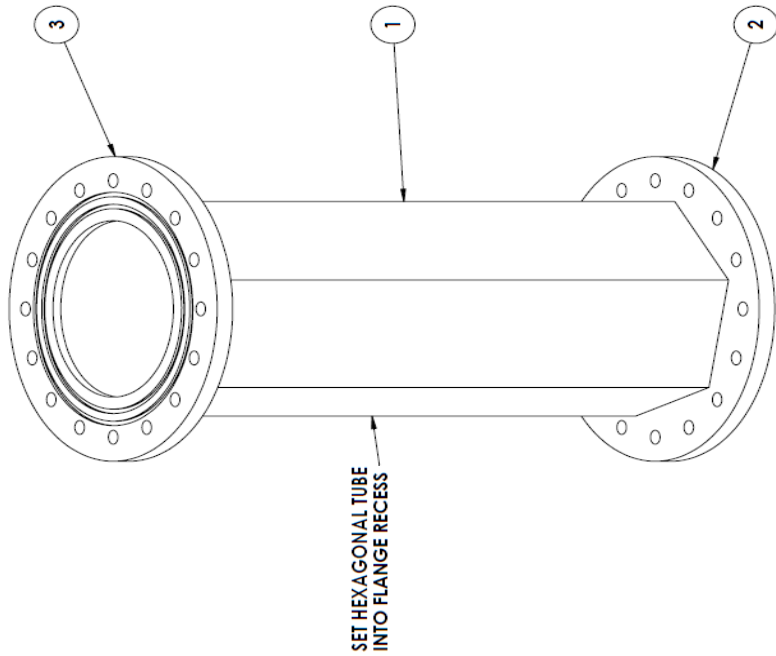
APPENDIX A.

MIR FACILITY DRAWINGS

This appendix includes the preliminary drawings created for the MIR facility. Some changes were later made but were not changed in the drawings. The main changes consisted of the removal of the stabilizing rings on the reducer flange and an increase in flange thickness for the diffuser and reducer. The increase in flange thickness was decided upon after the fabrication company suggested it in order to avoid bowing of the material during the welding process.

4 3 2 1

REVISIONS			
ZONE	REV.	DESCRIPTION	DATE
			APPROVED



ITEM NO.	PART NUMBER	DESCRIPTION	QTY.
1	Hexagonal Tube		1
2	Flange	Flat Flange	1
3	Flange	O Ring Flange	1

UNLESS OTHERWISE SPECIFIED:
 DIMENSIONS ARE IN INCHES
 TOLERANCES:
 FRACTIONAL DECIMALS .015, .030, .063, .125
 TWO PLACE DECIMAL .005, .010, .020, .040, .080
 THREE PLACE DECIMAL .001, .002, .005, .010, .020, .040, .080
 INTERFERE GEOMETRIC TOLERANCING PER COMMENTS
 MATERIAL FINISH

DO NOT SCALE DRAWING

SCALE: 1:20/WEIGHT: SHEET 1 OF 16

TITLE:
HEXAGONAL TUBE ASSEMBLY

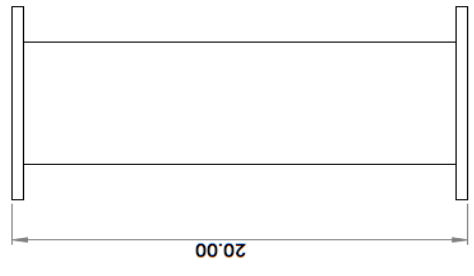
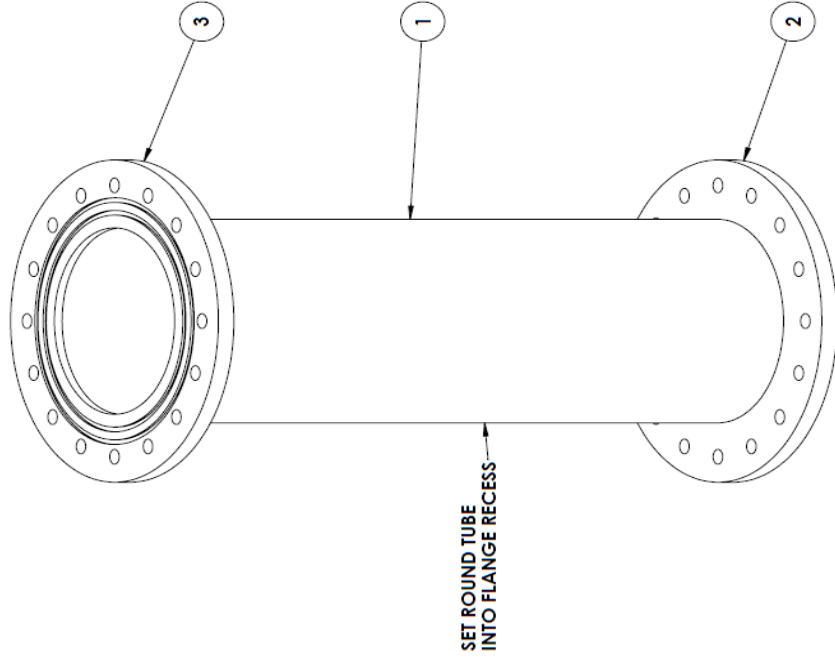
SIZE	DWG. NO.	REV
B	No. Bed Column Assembly	

SOLIDWORKS Educational Product. For Instructional Use Only

4 3 2 1

4 3 2 1

REVISIONS			
ZONE	REV.	DESCRIPTION	DATE



ITEM NO.	PART NUMBER	DESCRIPTION	20in Round Tube Assembly/QTY.
1	Round Tube	19.5in Round Tube	1
2	Flange	Flat Flange	1
3	Flange	O Ring Flange	1

UNLESS OTHERWISE SPECIFIED:		NAME	DATE
DIMENSIONS ARE IN INCHES		DRAWN	
TOLERANCES:		CHECKED	
FRACTIONS ALL		ENG. APPR.	
TENTHS		MFG. APPR.	
TWO PLACE DECIMAL		Q.A.	
THREE PLACE DECIMAL		COMMENTS:	
TOLERANCING PER:			
MATERIAL:			
FINISH:			

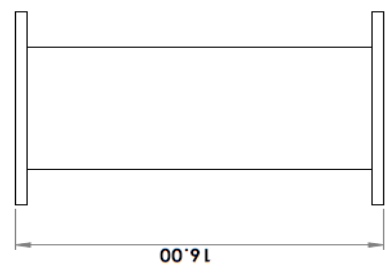
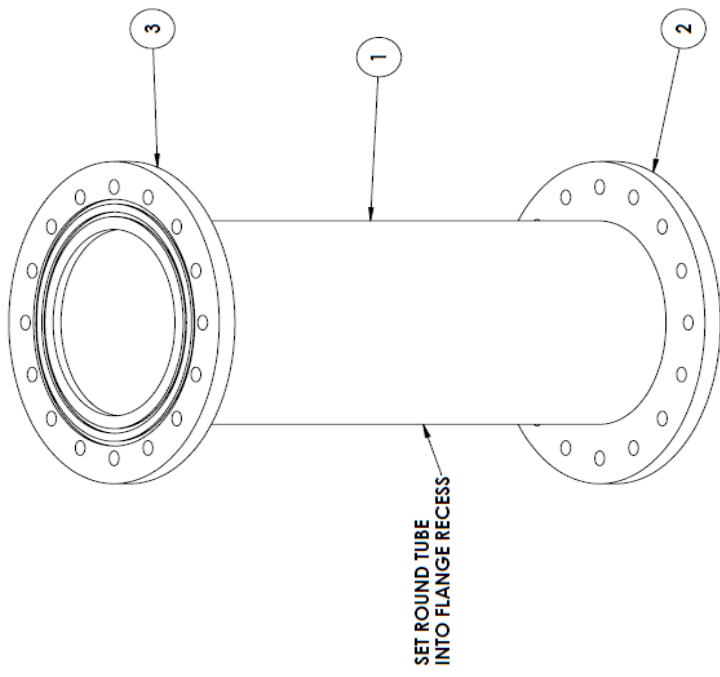
TITLE:		SIZE	DWG. NO.	REV
LONG ROUND TUBE ASSEMBLY		B	Pebble Bed Column Assembly	
SCALE: 1:20/WEIGHT:				SHEET 2 OF 16

SOLIDWORKS Educational Product. For Instructional Use Only

4 3 2 1

4 3 2 1

REVISIONS			
ZONE	REV.	DESCRIPTION	DATE
			APPROVED



ITEM NO.	PART NUMBER	DESCRIPTION	16in Round Tube Assembly/Qty
1	Round Tube	15.5in Round Tube	1
2	Flange	Flat Flange	1
3	Flange	O Ring Flange	1

UNLESS OTHERWISE SPECIFIED:	NAME	DATE
DIMENSIONS ARE IN INCHES	DRAWN	
TOLERANCES:	CHECKED	
ANGULAR: MACH. ± 0.008	ENG. APPR.	
TWO PLACE DECIMAL ± 0.008	MFG. APPR.	
THREE PLACE DECIMAL ± 0.0008		
INTERPRET GEOMETRIC TOLERANCING PER:	O.A.	
MATERIAL:	COMMENTS:	
FINISH:		

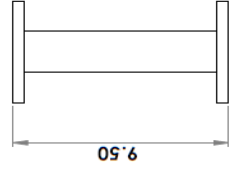
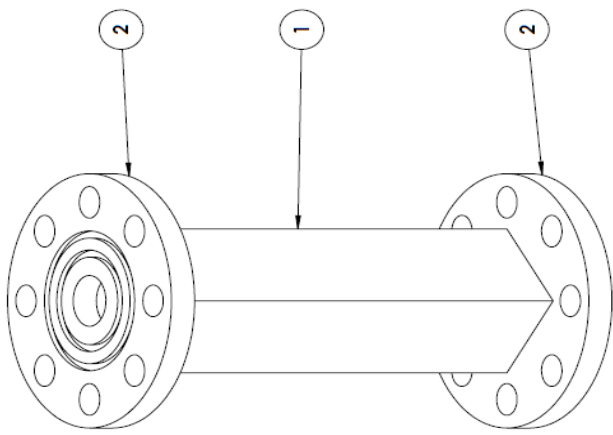
TITLE:		SIZE	DWG. NO.	REV
LONG ROUND TUBE ASSEMBLY		B	Pebble Bed Column Assembly	
DO NOT SCALE DRAWING		SCALE: 1:20 WEIGHT:		SHEET 3 OF 16

SOLIDWORKS Educational Product. For Instructional Use Only

4 3 2 1

4 3 2 1

REVISIONS				
ZONE	REV.	DESCRIPTION	DATE	APPROVED



B

B

A

A

ITEM NO.	PART NUMBER	DESCRIPTION	QTY.
1	Square Profile Center Tube		1
2	Small Flange		2

UNLESS OTHERWISE SPECIFIED:	NAME	DATE
DIMENSIONS ARE IN INCHES	DRAWN	
TOLERANCES:	CHECKED	
ANGLES: ±0.005	APPROVED	
ANGULAR MATCH: BEND ±	DATE	
TWO PLACE DECIMAL ± 0.005	ENG APPL.	
THREE PLACE DECIMAL ±	MFG APPL.	
INTERPRET GEOMETRIC TOLERANCING PER:	O.A.	
MATERIAL:	COMMENTS:	
FINISH:		

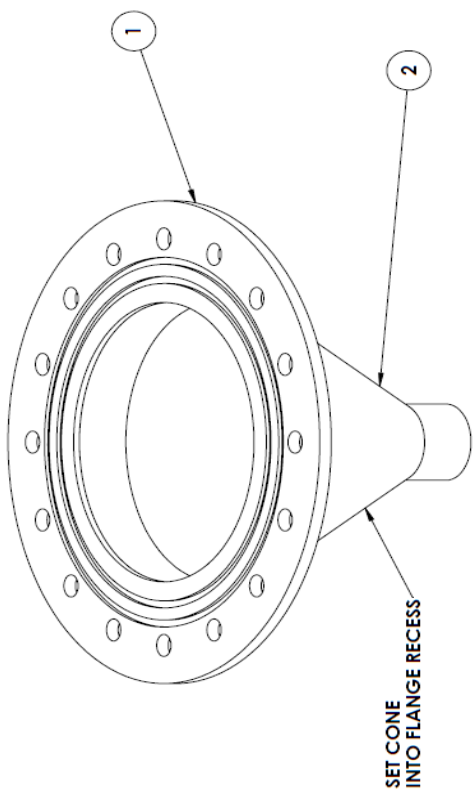
SIZE	DWG. NO.	REV
B	Pebble Bed Column Assembly	
SCALE: 1:2	WEIGHT:	SHEET 4 OF 16

SOLIDWORKS Educational Product. For Instructional Use Only

4 3 2 1

4 3 2 1

REVISIONS			
ZONE	REV.	DESCRIPTION	DATE
			APPROVED



B

A

ITEM NO.	PART NUMBER	DESCRIPTION	QTY.
1	Flange	Diffuser Flange	1
2	Cone		1

UNLESS OTHERWISE SPECIFIED:	NAME	DATE
DIMENSIONS ARE IN INCHES	DRAWN	
TOLERANCES:	CHECKED	
FRACTIONALS .0004 .0005 .0008	ENG. APPR.	
TWO PLACE DECIMAL .0008	MFG APPR.	
THREE PLACE DECIMAL .0008	G.A.	
INTERFER GEOMETRIC TOLERANCING PER:	COMMENTS:	
MATERIAL:		
FINISH:		

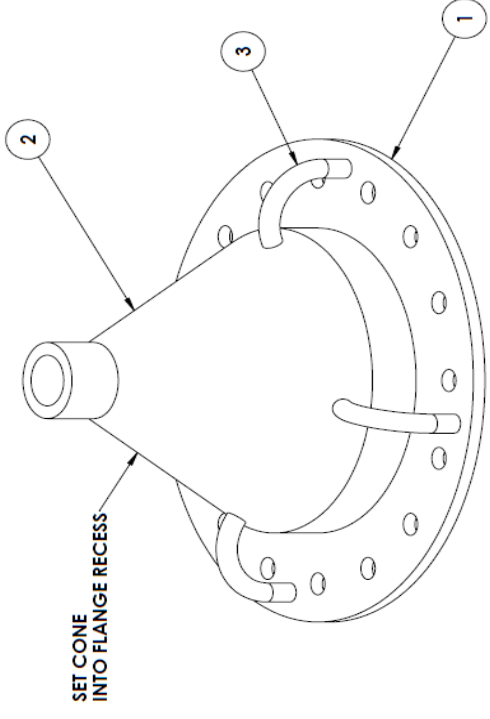
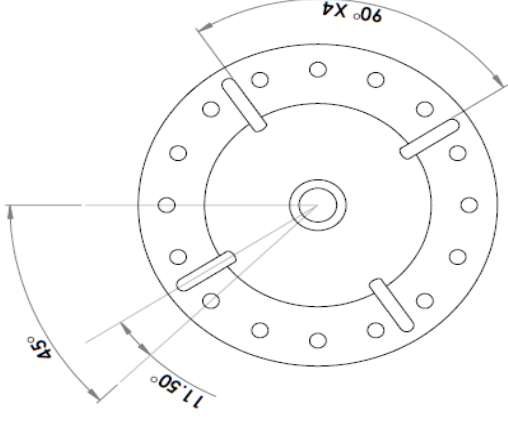
TITLE: DIFFUSER ASSEMBLY	
SIZE	DWG. NO.
B	Pebble-Bed Column Assembly
SCALE: 1:20	WEIGHT: SHEET 5 OF 16

SOLIDWORKS Educational Product. For Instructional Use Only

4 3 2 1

4 3 2 1

REVISIONS				
ZONE	REV.	DESCRIPTION	DATE	APPROVED



ITEM NO.	PART NUMBER	DESCRIPTION	QTY.
1	Flange	Reducer Flange	1
2	Cone		1
3	Stabilizer Ring		4

UNLESS OTHERWISE SPECIFIED:	NAME	DATE
DRAWN		
CHECKED		
APPROVED		
MATERIAL		
TOLERANCES ARE IN INCHES		
FRACTIONS: 1/8, 1/4, 3/8, 1/2, 5/8, 3/4, 7/8		
DECIMALS: .125, .25, .375, .5, .625, .75, .875, 1.0		
ANGULAR DIMENSIONS: 1/4, 1/2, 3/4, 1, 1 1/4, 1 1/2, 1 3/4, 2, 2 1/4, 2 1/2, 2 3/4, 3, 3 1/4, 3 1/2, 3 3/4, 4, 4 1/4, 4 1/2, 4 3/4, 5, 5 1/4, 5 1/2, 5 3/4, 6, 6 1/4, 6 1/2, 6 3/4, 7, 7 1/4, 7 1/2, 7 3/4, 8, 8 1/4, 8 1/2, 8 3/4, 9, 9 1/4, 9 1/2, 9 3/4, 10		
TWO PLACE DECIMAL: .01, .02, .03, .04, .05, .06, .07, .08, .09, .10, .11, .12, .13, .14, .15, .16, .17, .18, .19, .20, .21, .22, .23, .24, .25, .26, .27, .28, .29, .30, .31, .32, .33, .34, .35, .36, .37, .38, .39, .40, .41, .42, .43, .44, .45, .46, .47, .48, .49, .50, .51, .52, .53, .54, .55, .56, .57, .58, .59, .60, .61, .62, .63, .64, .65, .66, .67, .68, .69, .70, .71, .72, .73, .74, .75, .76, .77, .78, .79, .80, .81, .82, .83, .84, .85, .86, .87, .88, .89, .90, .91, .92, .93, .94, .95, .96, .97, .98, .99, 1.00		
THREE PLACE DECIMAL: .001, .002, .003, .004, .005, .006, .007, .008, .009, .010, .011, .012, .013, .014, .015, .016, .017, .018, .019, .020, .021, .022, .023, .024, .025, .026, .027, .028, .029, .030, .031, .032, .033, .034, .035, .036, .037, .038, .039, .040, .041, .042, .043, .044, .045, .046, .047, .048, .049, .050, .051, .052, .053, .054, .055, .056, .057, .058, .059, .060, .061, .062, .063, .064, .065, .066, .067, .068, .069, .070, .071, .072, .073, .074, .075, .076, .077, .078, .079, .080, .081, .082, .083, .084, .085, .086, .087, .088, .089, .090, .091, .092, .093, .094, .095, .096, .097, .098, .099, 1.000		
INTERPRET GEOMETRIC TOLERANCING PER:		
COMMENTS:		
MATERIAL:		
FINISH:		
DO NOT SCALE DRAWING		

TITLE: REDUCER ASSEMBLY

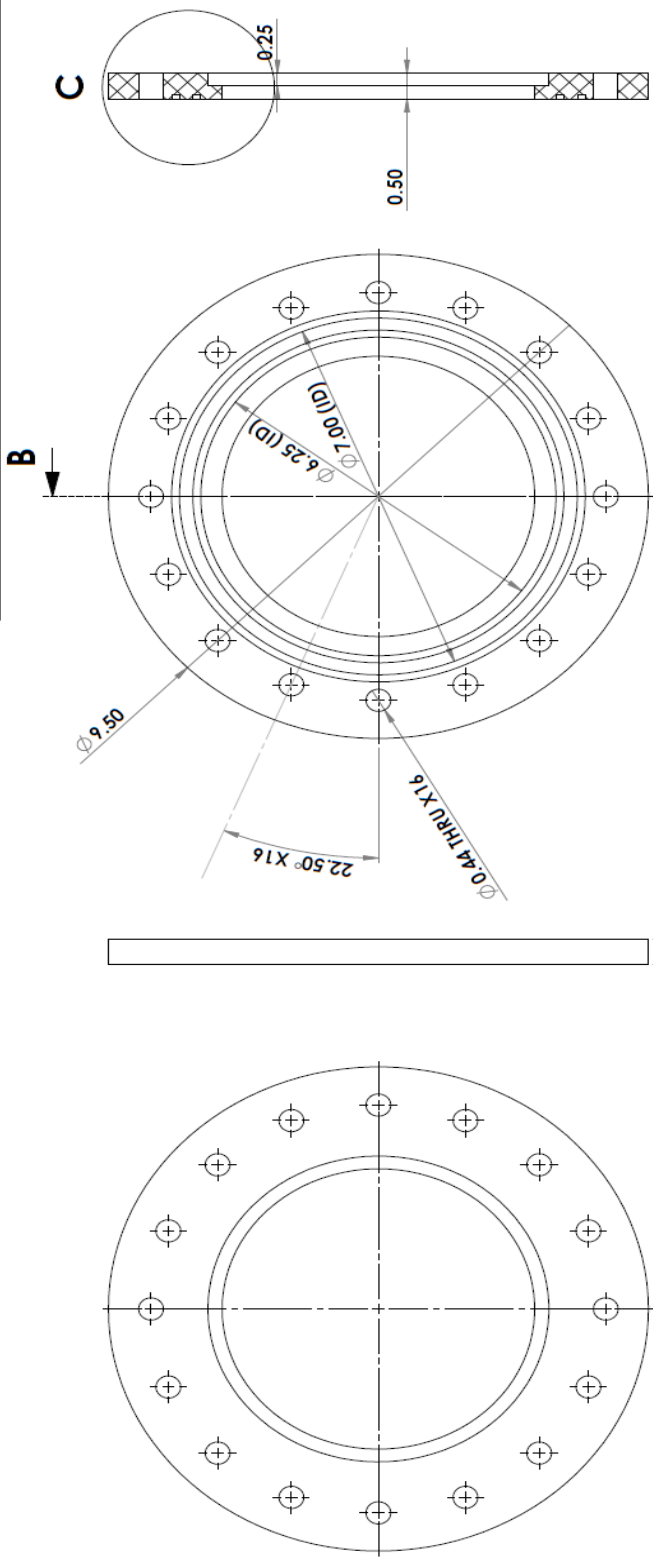
SIZE	DWG. NO.	REV
B	Pebble Bed Column Assembly	
SCALE: 1:20	WEIGHT:	SHEET 6 OF 16

SOLIDWORKS Educational Product. For Instructional Use Only

4 3 2 1

1 2 3 4

REVISIONS			DATE	APPROVED
ZONE	REV.	DESCRIPTION		



SECTION B-B

UNLESS OTHERWISE SPECIFIED:	DRAWN	DATE
TOLERANCES ARE IN INCHES:	CHECKED	
FRACTIONAL CHA. BING 4.	ENG. APPL.	
TWO PLACE DECIMAL ± 0.005	MFG. APPL.	
THREE PLACE DECIMAL ± 0.001	O.A.	
INTERPRET GEOMETRIC TOLERANCING PER:	COMMENT:	
MATERIAL:		
FINISH:		
DO NOT SCALE DRAWING		

TITLE: **O-RING FLANGE**

SIZE: DWG. NO. **B** Pebble Bed Column Assembly

REV: **1**

SCALE: 1:2 WEIGHT: SHEET 7 OF 16

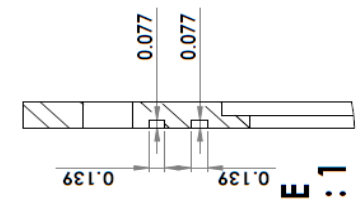
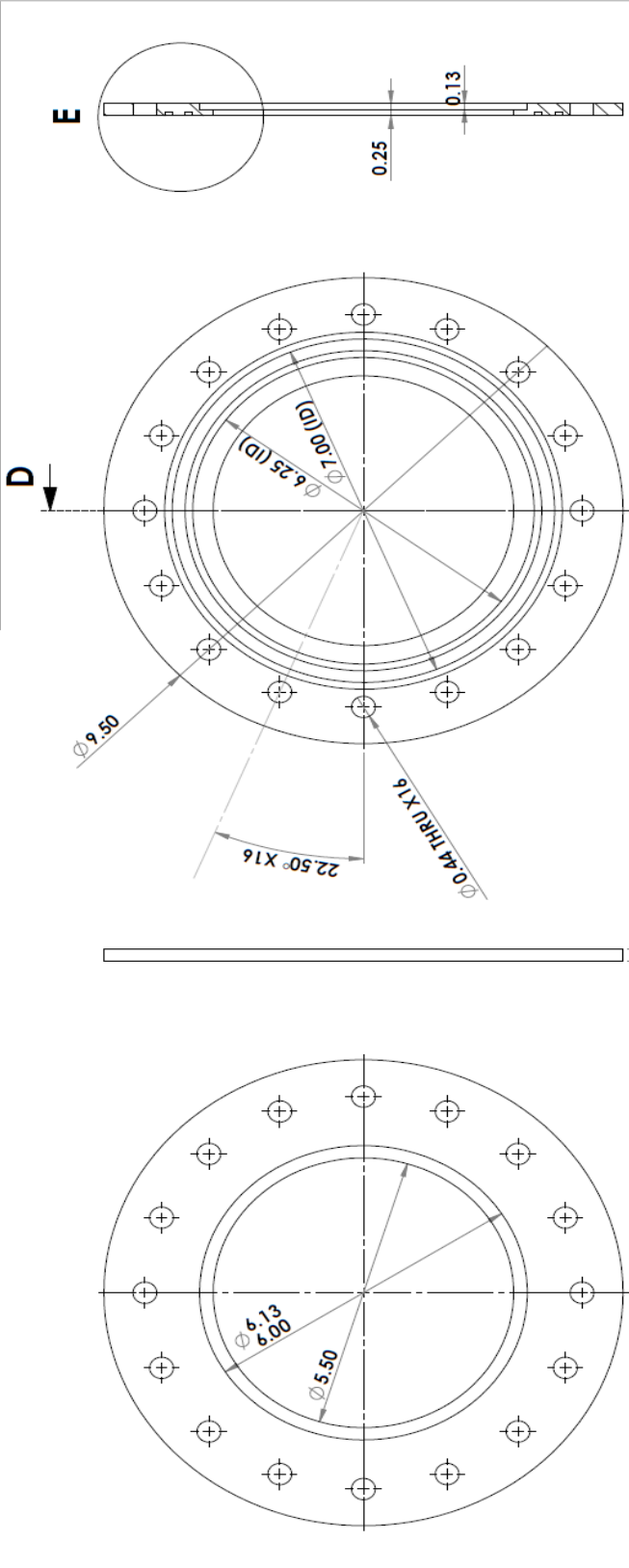
DETAIL C
SCALE 1:1

SOLIDWORKS Educational Product. For Instructional Use Only

1 2 3 4

1 2 3 4

REVISIONS			
ZONE	REV.	DESCRIPTION	DATE



SECTION D-D

UNLESS OTHERWISE SPECIFIED:	NAME	DATE
DIMENSIONS ARE IN INCHES	DRAWN	
TOLERANCES:	CHECKED	
ANGULAR MATCH - BEND \pm	ENG APPL	
TWO PLACE DECIMAL ± 0.005		
THREE PLACE DECIMAL ± 0.010		
INTERPRET GEOMETRIC TOLERANCING PER:	O.A.	
MATERIAL	COMMENTS:	
FINISH		

TITLE: DIFFUSER FLANGE

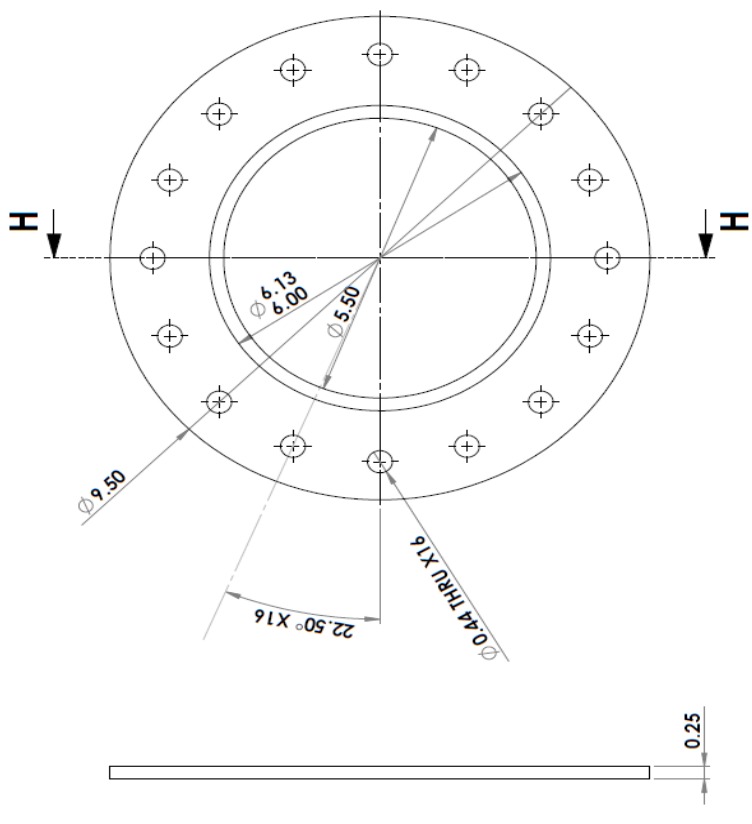
SIZE DWG. NO. Pebble Red Column Assembly
B REV
 SCALE: 1:2 WEIGHT: SHEET 8 OF 16

SOLIDWORKS Educational Product. For Instructional Use Only

1 2 3 4

1 2 3 4

REVISIONS				
ZONE	REV.	DESCRIPTION	DATE	APPROVED



SECTION H-H

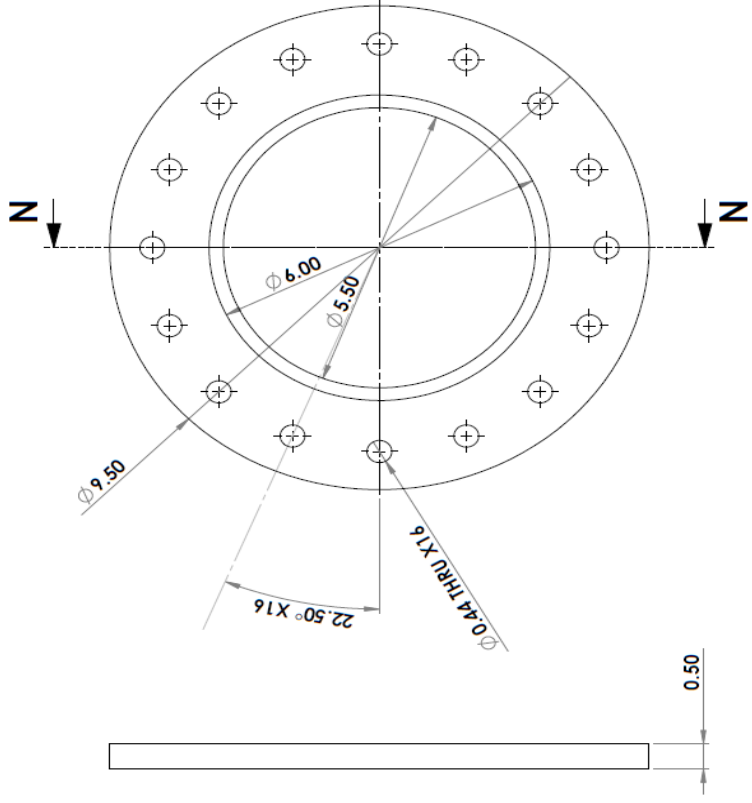
UNLESS OTHERWISE SPECIFIED: DIMENSIONS ARE IN INCHES TOLERANCES: FRACTIONS ALL DECIMALS TO .0004 - BOND 4 TWO PLACE DECIMAL - 1.0 USR THREE PLACE DECIMAL - 3 INTERPRET GEOMETRIC TOLERANCING PER MATERIAL	DRAWN CHECKED ENG. APPR. MFG APPR. G.A. COMMENTS:	NAME DATE	TITLE: REDUCER FLANGE
DO NOT SCALE DRAWING	SIZE DWG. NO. B	PEBBLE BED COLUMN ASSEMBLY	REV
	SCALE: 1:2	WEIGHT:	SHEET 9 OF 16

SOLIDWORKS Educational Product. For Instructional Use Only

1 2 3 4

1 2 3 4

REVISIONS				
ZONE	REV.	DESCRIPTION	DATE	APPROVED



SECTION N-N

UNLESS OTHERWISE SPECIFIED:	NAME	DATE
DIMENSIONS ARE IN INCHES	DRAWN	
TOLERANCES:	CHECKED	
ANGULAR MATCH: BEND \pm	ENG APPL	
TWO PLACE DECIMAL ± 0.005	MFG APPL	
THREE PLACE DECIMAL \pm	O.A.	
INTERPRET GEOMETRIC TOLERANCING PER:	COMMENTS:	
MATERIAL:		
FINISH:		
DO NOT SCALE DRAWING		

TITLE: **FLAT FLANGE**

SIZE DWG. NO. **B** Pebble Bed Column Assembly

SCALE: 1:2 WEIGHT: **1**

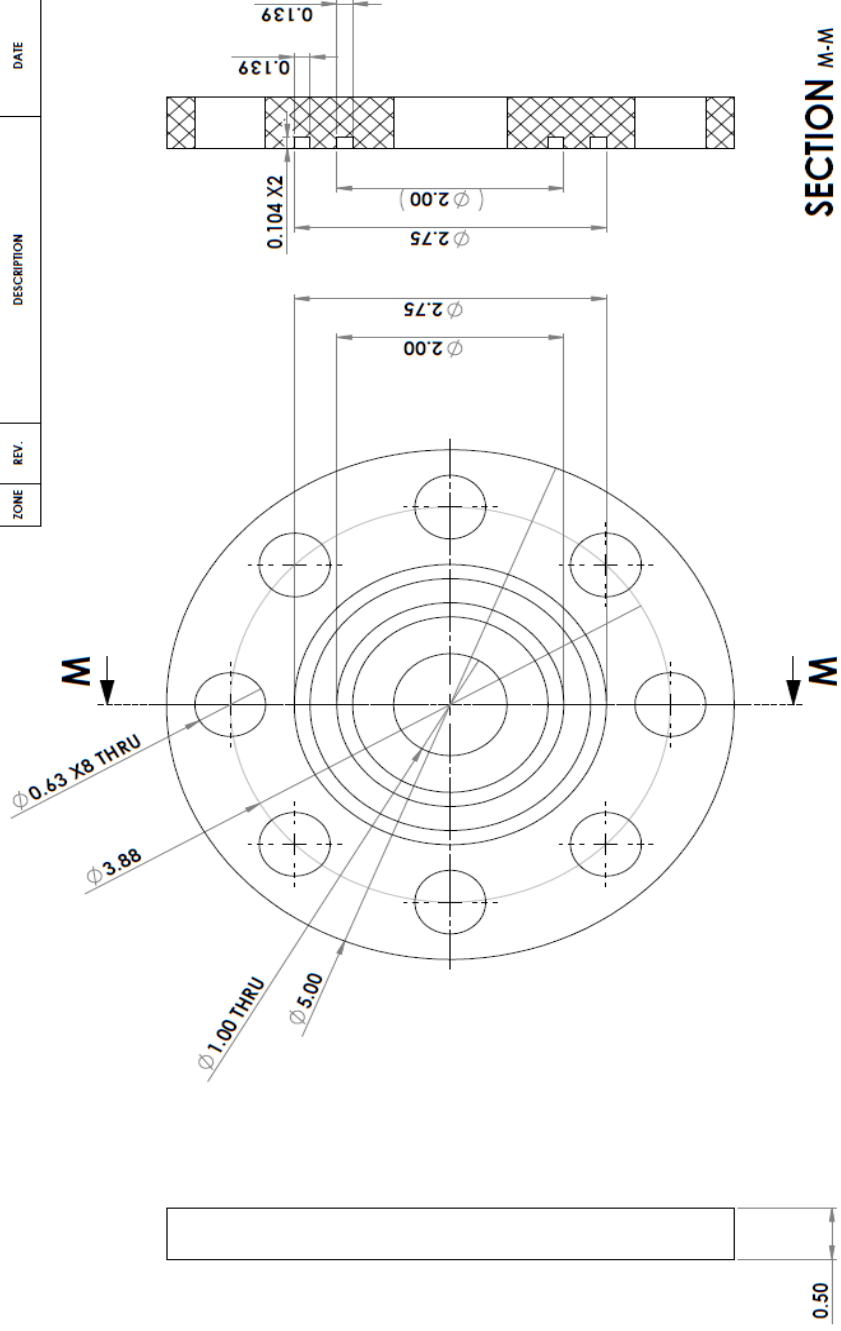
SHEET 10 OF 13

SOLIDWORKS Educational Product. For Instructional Use Only

1 2 3 4

1 2 3 4

REVISIONS			
ZONE	REV.	DESCRIPTION	DATE



SECTION M-M

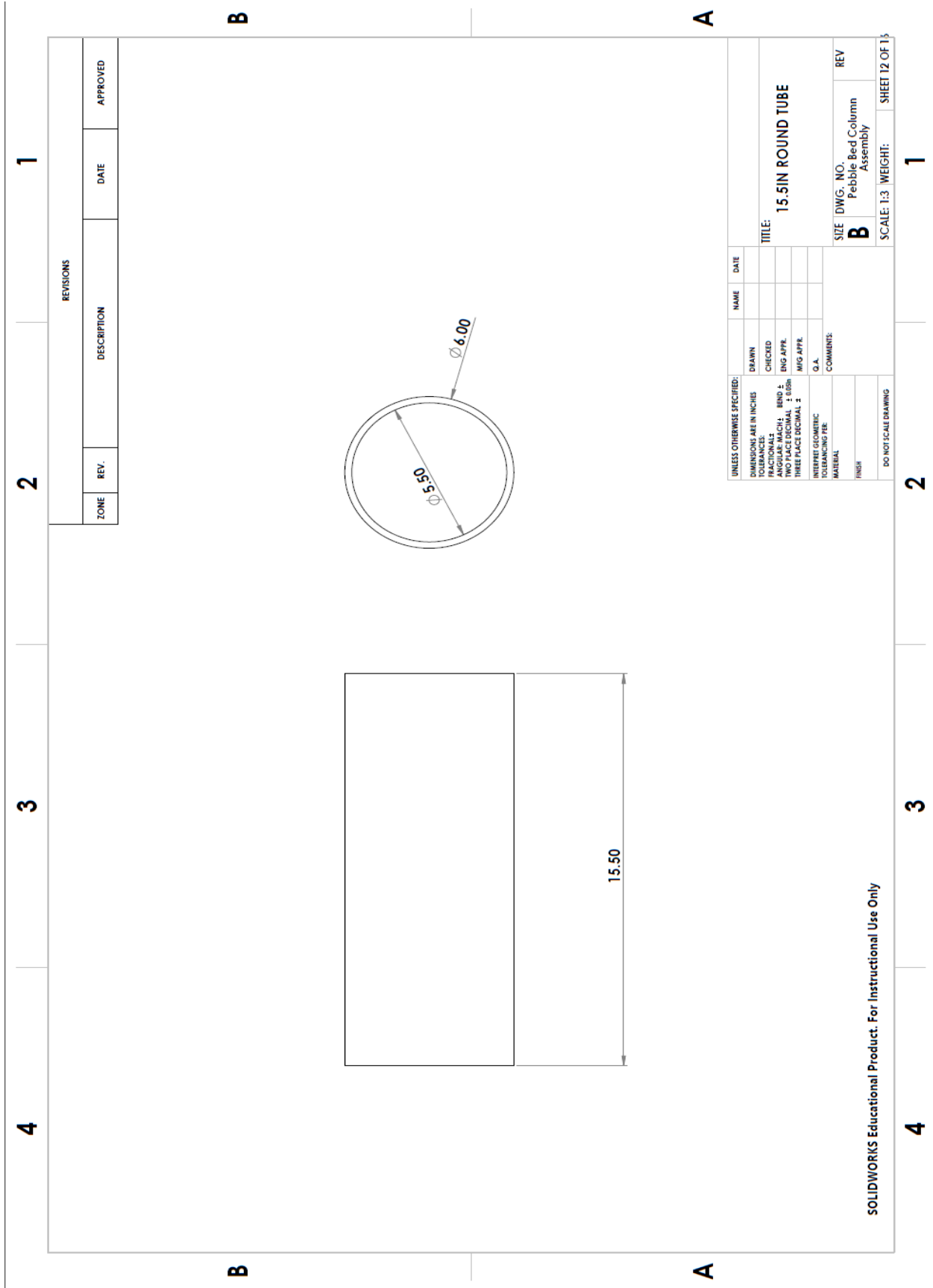
UNLESS OTHERWISE SPECIFIED:	NAME	DATE
DIMENSIONS ARE IN INCHES	DRAWN	
TOLERANCES:	CHECKED	
ANGULAR DIMS: BEND ±	ENG APPL	
ANGULAR DIMS: BEND ±	AWG APPL	
TWO PLACE DECIMAL ± 0.005	O.A.	
THREE PLACE DECIMAL ±	COMMENTS:	
INTERPRET GEOMETRIC TOLERANCING PER:	MATERIAL:	
FINISH:		
DO NOT SCALE DRAWING		

TITLE: SMALL FLANGE

SIZE	DWG. NO.	REV
B	Pebble Bed Column Assembly	
SCALE: 1:1	WEIGHT:	SHEET 11 OF 13

SOLIDWORKS Educational Product. For Instructional Use Only

1 2 3 4



REVISIONS			
ZONE	REV.	DESCRIPTION	DATE
			APPROVED

UNLESS OTHERWISE SPECIFIED:	NAME	DATE
DIMENSIONS ARE IN INCHES		
TOLERANCES:		
FRACTIONAL	DRAWN	
DECIMAL	CHECKED	
TWO PLACE DECIMAL	ENG. APPL.	
THREE PLACE DECIMAL	MFG. APPL.	
	Q.A.	
INTERFERE GEOMETRIC	COMMENT:	
TOLERANCING PER		
MATERIAL		
FINISH		
DO NOT SCALE DRAWING		

TITLE: **15.5 IN ROUND TUBE**

SIZE DWG. NO. **B** Pebble Bed Column Assembly

SCALE: 1:3 WEIGHT: **1**

SHEET 12 OF 15

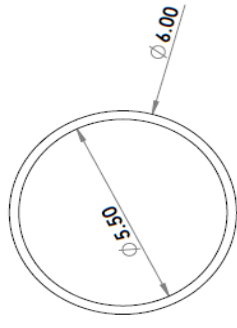
SOLIDWORKS Educational Product. For Instructional Use Only

4 3 2 1

REVISIONS			
ZONE	REV.	DESCRIPTION	DATE

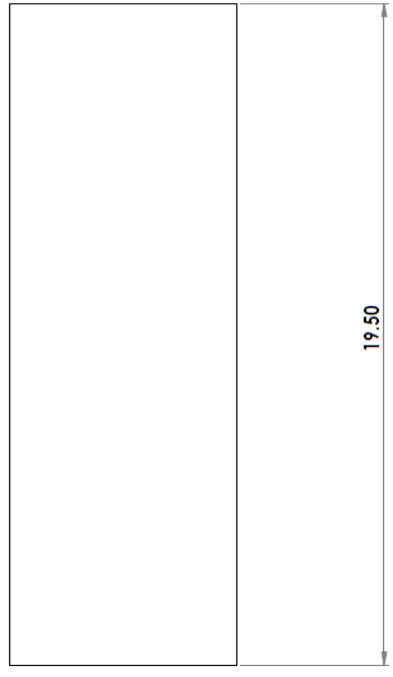
B

B



A

A



UNLESS OTHERWISE SPECIFIED:		NAME	DATE
DIMENSIONS ARE IN INCHES	DRAWN		
TOLERANCES:	CHECKED		
ANGULAR: MACH.	ENG. APPL.		
TWO PLACE DECIMAL	MFG. APPL.		
THREE PLACE DECIMAL	O.A.		
INTERPRET GEOMETRIC TOLERANCING PER:	COMMENTS:		
MATERIAL:			
FINISH:			

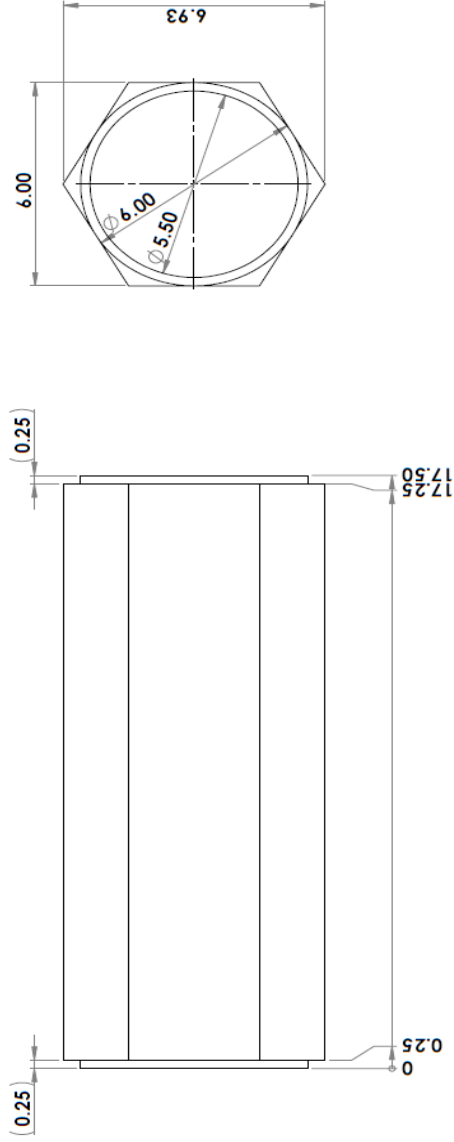
TITLE: 19.5IN ROUND TUBE
 SIZE DWG. NO. B
 Pebble Bed Column Assembly
 SCALE: 1:3 WEIGHT: SHEET 13 OF 13

SOLIDWORKS Educational Product. For Instructional Use Only

4 3 2 1

4 3 2 1

REVISIONS				
ZONE	REV.	DESCRIPTION	DATE	APPROVED



B

A

UNLESS OTHERWISE SPECIFIED:	NAME	DATE
DIMENSIONS ARE IN INCHES	DRAWN	
TOLERANCES:	CHECKED	
ANGLES: MACH.	ENG. APPL.	
TWO PLACE DECIMAL ± 0.005	MFG. APPL.	
THREE PLACE DECIMAL ±		
INTERPRET GEOMETRIC TOLERANCING PER:	O.A.	
MATERIAL:	COMMENTS:	
FINISH:		
DO NOT SCALE DRAWING		

TITLE: HEXAGONAL TUBE

SIZE	DWG. NO.	REV
B	Pebble Red Column Assembly	
SCALE: 1:3	WEIGHT:	SHEET 14 OF 15

4 3 2 1

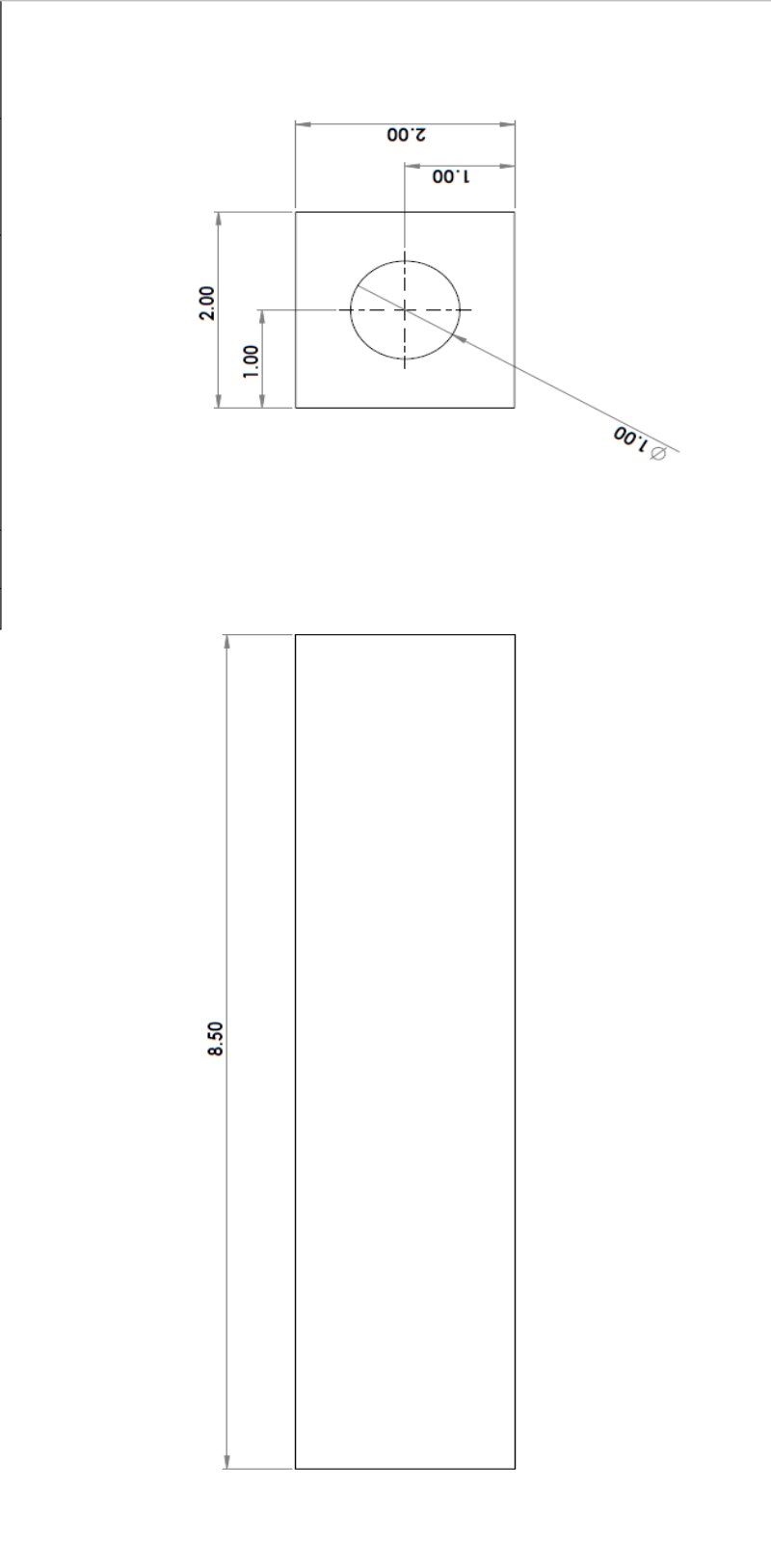
B

A

SOLIDWORKS Educational Product. For Instructional Use Only

4 3 2 1

REVISIONS			
ZONE	REV.	DESCRIPTION	DATE



UNLESS OTHERWISE SPECIFIED: DIMENSIONS ARE IN INCHES TOLERANCES: FRACTIONS: FURNISH AS SHOWN DECIMALS: FURNISH AS SHOWN TWO PLACE DECIMAL ± 0.005 THREE PLACE DECIMAL ± 0.001	DRAWN CHECKED ENG. APPL. MFG. APPL. O.A. COMMENTS:	NAME DATE
TITLE: SQUARE PROFILE TUBE		
SIZE DWG. NO. B Pebble Bed Column Assembly		
SCALE: 1:1 WEIGHT: 1		
DO NOT SCALE DRAWING		
SHEET 15 OF 15		

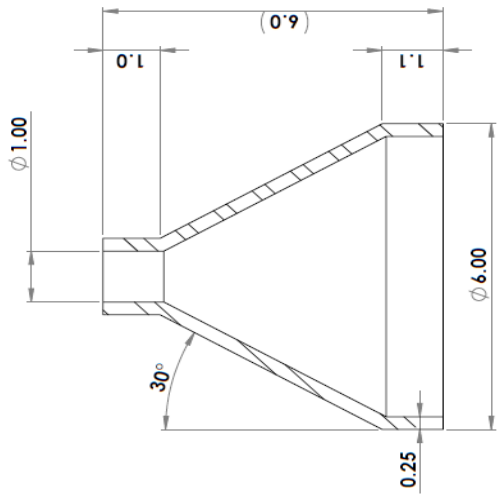
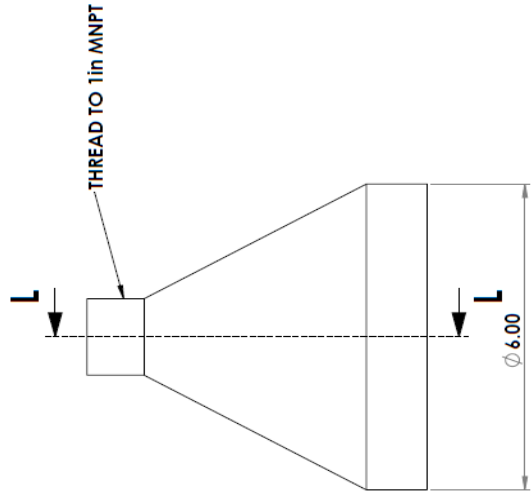
SOLIDWORKS Educational Product. For Instructional Use Only

4 3 2 1

4 3 2 1

REVISIONS			
ZONE	REV.	DESCRIPTION	DATE

B B



SECTION L-L

A A

UNLESS OTHERWISE SPECIFIED:	NAME	DATE
DIMENSIONS ARE IN INCHES	DRAWN	
TOLERANCES:	CHECKED	
FRACTIONS TO NEAREST 1/32	ENG APPR.	
DECIMALS TO NEAREST 0.0005	MFG APPR.	
TWO PLACE DECIMAL 0.0005	O.A.	
THREE PLACE DECIMAL 0.0001	COMMENTS:	
INTERPRET GEOMETRIC TOLERANCING PER:		
MATERIAL:		
FINISH:		
DO NOT SCALE DRAWING		

TITLE:		CONE	
SIZE	DWG. NO.	REV	
B	Pebble Bed Column Assembly		
SCALE: 1:2	WEIGHT:	SHEET 16 OF 15	

4 3 2 1

SOLIDWORKS Educational Product. For Instructional Use Only

APPENDIX B.

PEBBLE CENTROID LOCATIONS LIST

This Appendix contains the centroid locations for the second experimental facility pebble bed scan conducted. The table of centroid locations calculated for the spheres within the experimental test section can be seen below in Table B.1. The “T/B” column represents the whether the sphere cross-section was determined to be the from on Top or Bottom of the sphere’s centroid. Those spheres with the capability of being measured in multiple images had the measurements averaged and are labeled “ave.”

Table B.1: Centroid listing for spheres in experimental facility two

Sphere	Top/bottom	X distance [in]	Y distance [in]	Z distance [in]
1	T	1.849276034	0.623819481	-0.056077627
2	T	2.71242293	0.43777512	0.066601363
3	T	3.565259469	0.585924355	-0.08438627
4	T	0.732266702	1.588616695	-0.324889598
5	T	1.568065073	1.470709659	-0.032764383
6	B	2.420182224	1.257090923	0.179516416
7	B	3.267654626	1.307598608	0.332381055
8	B	4.251418431	0.988553745	0.294180019
9	B	0.484392859	2.286030445	0.227038132
10	ave	1.360990909	2.263375583	0.298379087
11	B	2.294865756	2.098685223	0.334039377
12	T	2.932831808	2.050694491	-0.307075001
13	T	3.91889861	1.682954298	-0.131319149
14	T	4.783440204	1.649106916	-0.149493054
15	B	0.523569934	3.368724127	0.271481752
16	T	1.823919008	3.086066841	0.038999021
17	T	2.637861287	2.876467933	-0.200933635
18	T	3.600652372	2.488787186	0.065384542
19	B	4.426562298	2.302633376	0.298601781
20	T	5.052037746	2.463448376	-0.335282369
21	T	0.818744873	4.027696566	-0.26772604

22	ave	1.411456966	3.82044688	0.312579278
23	T	2.050797769	3.878271825	-0.261275715
24	T	2.907150611	3.725889786	-0.322047344
25	B	3.392200172	3.302267547	0.282861145
26	T	4.237281249	3.060275033	-0.09946257
27	B	5.054141569	2.983786279	0.354569066
28	T	4.959535291	3.484684108	-0.343370051
29	B	1.609602386	4.756693302	0.314149809
30	T	2.192881972	5.003709573	-0.26999448
31	T	2.861612495	4.514752561	0.03417603
32	T	3.712337732	4.293624234	0.025338929
33	T	4.572901927	4.171833457	-0.00315068
34	B	0.782475653	1.524273157	0.524124842
35	B	2.55179424	3.370187286	0.510404996
36	B	2.227023528	4.177788455	0.524069585
37	T	4.137559997	3.663868693	0.529024806
38	B	2.403346193	5.030416002	0.568571954
39	T	3.449549015	4.967280403	0.506442044
40	B	1.373480265	0.890152147	0.614393243
41	B	1.239822379	3.0442196	0.678148525
42	B	2.950194526	2.592980225	0.627846632
43	T	3.204405279	4.053163829	0.690009062
44	B	2.158016901	0.507992826	0.74638358
45	B	3.274497108	0.497688577	0.736068471
46	T	3.742355982	1.946732974	0.71550652
47	T	4.719911625	1.542069599	0.787089532
48	T	3.927628889	2.852235282	0.790486705
49	T	4.197168221	4.557030102	0.678950526
50	B	1.717557641	1.670236061	0.819632013
51	B	0.434353949	2.810141682	0.919704354
52	B	2.050427207	2.765577797	0.865586023
53	T	5.030781099	2.346327369	0.951162365
54	T	1.102030801	4.379938511	0.914579569
55	B	2.47498581	1.282581792	1.019838869
56	T	4.691928305	3.997297064	1.113400291
57	T	4.014599946	0.8161705	1.099870927
58	T	0.635458355	3.675437417	1.079946658
59	T	1.751815929	3.625114659	1.114253345
60	B	4.673070855	3.119007034	1.129296295
61	T	1.793535887	4.859222264	1.186638334
62	B	2.907095874	4.703292271	1.188410465
63	T	0.554814031	2.007169885	1.27755893
64	T	1.351888289	2.368908194	1.247013594

65	B	2.615055072	2.118690111	1.256366224
66	T	2.580647098	3.854944828	1.264754708
67	B	3.826755648	3.961144449	1.310838881
68	B	2.714695753	0.438988681	1.41196171
69	T	0.987381834	1.254596405	1.36354568
70	T	4.132388671	1.620423791	1.442261498
71	T	3.398354515	2.491312525	1.391455953
72	B	3.753223295	4.828215366	1.385193207
73	B	1.672429688	0.702906658	1.429508359
74	T	1.165959905	3.167192333	1.569683312
75	T	2.561343843	3.028666228	1.552578952
76	B	1.911265675	1.518813476	1.665665
77	T	3.968942414	3.16712104	1.645782994
78	B	3.513836411	0.567760933	1.764206258
79	T	4.891038614	1.864962125	1.796698753
80	B	0.436547453	2.681495251	1.798752521
81	B	2.006466426	2.404112874	1.821095466
82	T	5.071338671	2.714305996	1.800174939
83	B	1.236739902	4.495638366	1.777767625
84	T	3.164133911	4.167156205	1.841613898
85	B	2.372937442	5.031410421	1.822798416
86	T	2.775354776	1.206128165	1.871160014
87	B	3.460238446	1.822623449	1.938116839
88	B	4.180327831	2.360478932	1.90077787
89	ave	2.060433364	4.219517042	1.852114816
90	T	4.910914742	3.567954401	1.868976537
91	T	4.373951075	4.406535642	1.831821397
92	B	0.695897659	1.694555291	2.048615212
93	T	4.246391923	0.987273801	2.018123331
94	T	0.69593307	3.829758859	1.951302837
95	B	1.235095256	1.001935429	2.142887584
96	B	1.21386452	2.550360447	2.173786105
97	B	2.947976074	2.507455824	2.129114837
98	B	3.048092268	3.377733854	2.184333241
99	B	3.217445861	5.016342683	2.06961963
100	B	2.172239816	3.437150124	2.221911155
101	B	1.535844686	1.775184148	2.436631518
102	B	3.517313618	1.140213577	2.487103648
103	B	1.323975916	3.400938772	2.399090419
104	T	3.745076418	2.90832515	2.449888333
105	B	1.75228634	4.8347233	2.397426194
106	B	2.98560345	0.446057162	2.45856594
107	B	2.241045439	1.269341669	2.558576203

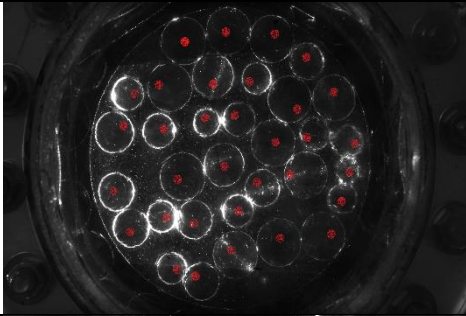
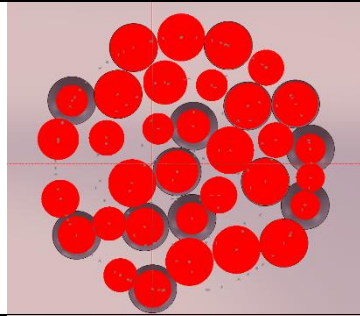
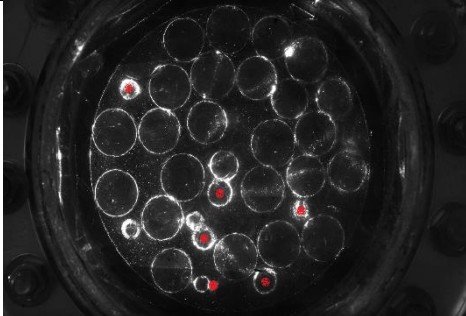
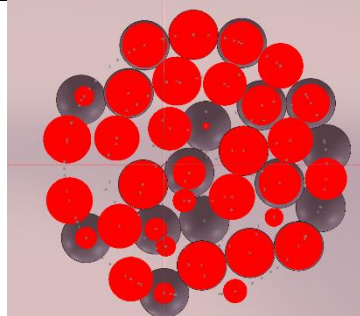
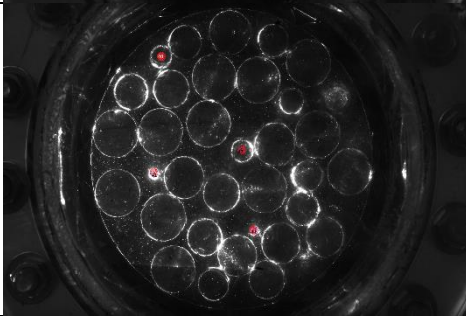
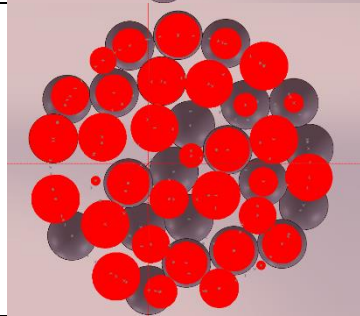
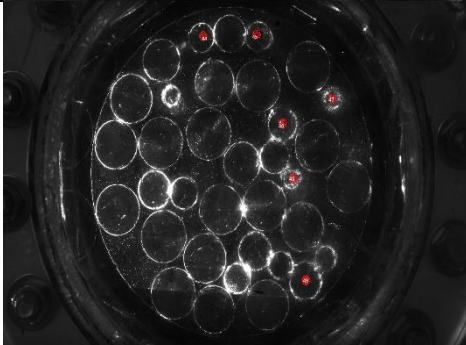
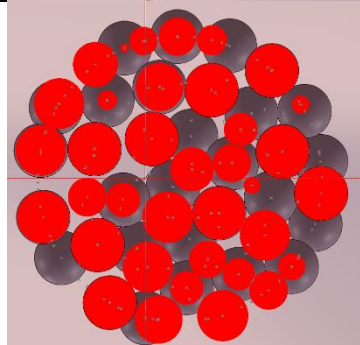
108	T	4.694267834	1.49222524	2.574240788
109	B	0.478038977	3.196605689	2.51701351
110	T	5.019408713	2.30518998	2.566438527
111	B	5.026807465	3.169054264	2.627287165
112	B	2.629262318	4.498253722	2.467582431
113	T	4.677860385	4.040929524	2.556417574
114	B	3.920880739	4.741938129	2.5131258
115	B	0.481267999	2.328059945	2.617336481
116	B	2.247758802	2.668264126	2.623848771
117	B	2.937720409	1.798581126	2.639375635
118	B	3.958872552	1.955727588	2.643742661
119	B	1.042451924	4.306336487	2.61022697
120	B	1.853337856	4.033090644	2.788709634
121	B	3.349631149	4.171860485	2.844496271
122	B	1.580565648	0.752415036	2.916125446
123	B	0.876445783	1.391723464	2.859520639
124	B	4.351853297	2.648694101	3.014439534
125	B	3.17412444	5.018778173	2.945809645
126	B	4.182199371	0.934225042	3.007852836
127	B	1.19924036	2.580510266	3.045576265
128	B	3.112166084	2.640450053	2.985970866
129	B	2.635179583	3.375097226	2.978683777
130	B	4.137160678	3.497572736	2.997834183
131	B	2.388223925	0.462617011	3.090971367
132	B	2.171810273	1.946215286	3.109036256
133	B	0.664725159	3.749179311	3.160091296
134	B	1.781181881	3.228904886	3.116800568
135	B	2.311111539	5.018112603	3.092753565
136	B	3.433814127	0.537132489	3.203232672
137	B	2.850275803	1.186273336	3.246193661
138	B	2.557852837	4.200970246	3.265524264
139	B	1.514986136	4.698905943	3.226613596
140	B	0.561000057	1.986059786	3.39290139
141	B	4.44457339	1.674541868	3.357077294
142	B	0.439524264	2.918665593	3.335913358
143	B	3.382723198	3.534597861	3.403529934
144	B	4.08607438	4.625776451	3.349366783
145	ave	3.262178256	3.307805717	1.129968018
146	ave	3.326833865	1.3509673	1.207912764
147	ave	2.189102669	0.509685639	2.121993575
148	ave	3.863375104	3.814764368	2.227828161

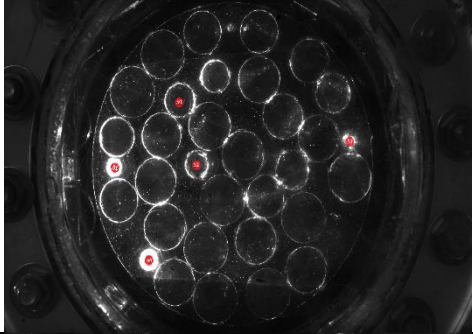
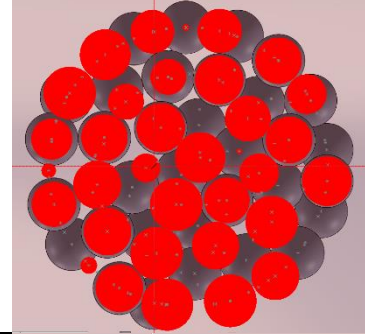
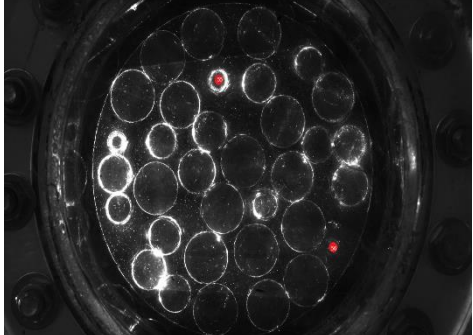
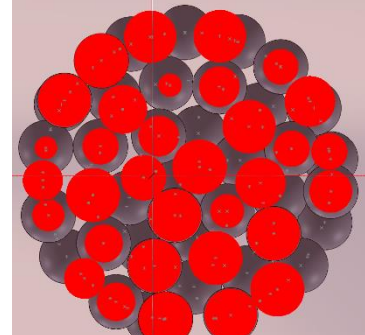
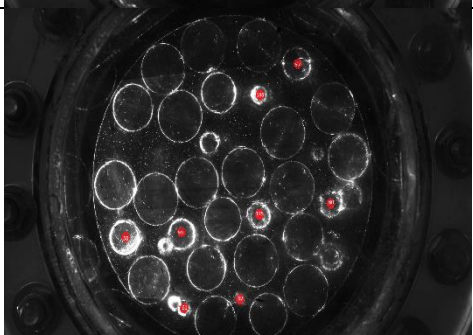
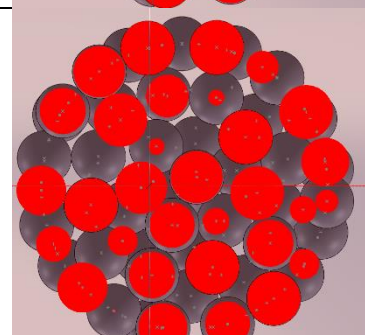
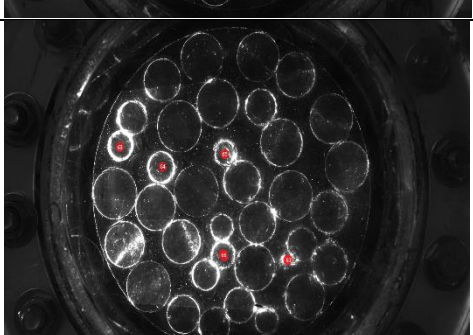
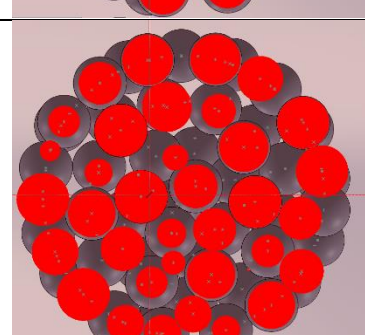
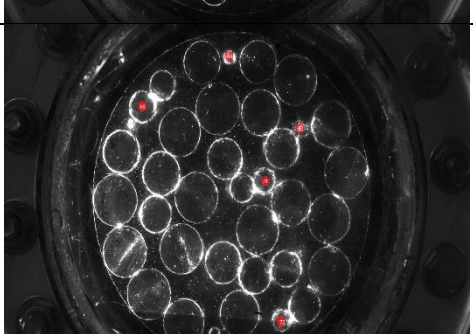
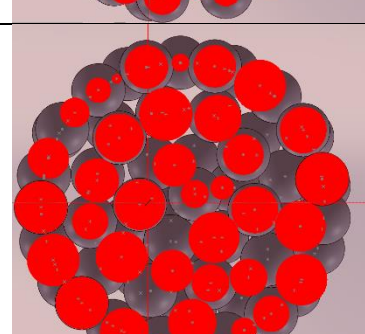
APPENDIX C.

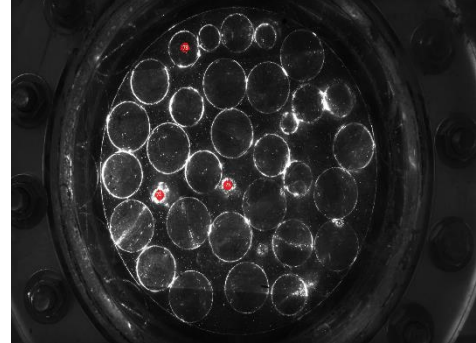
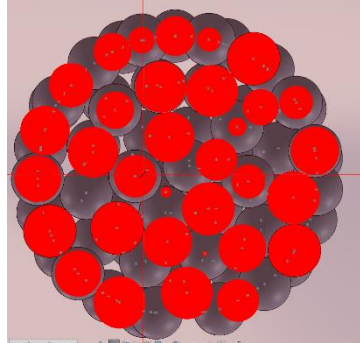
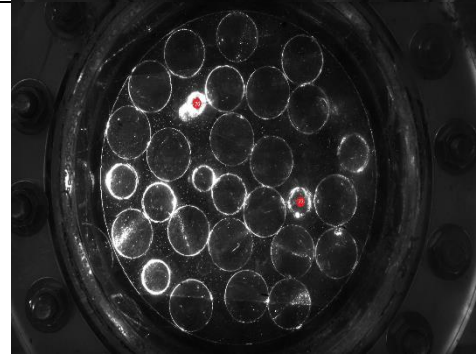
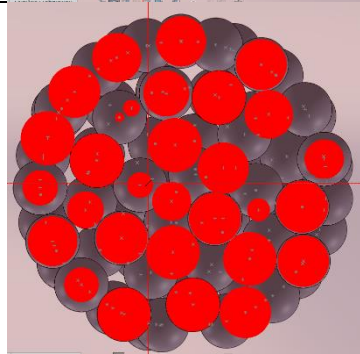
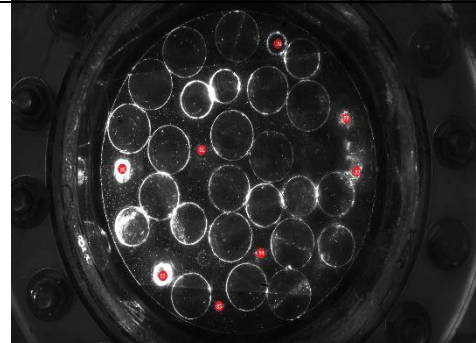
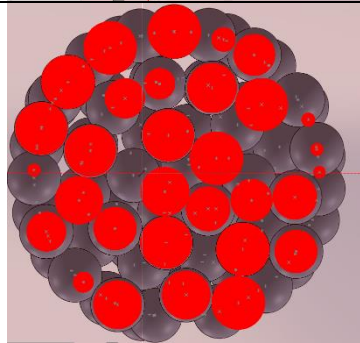
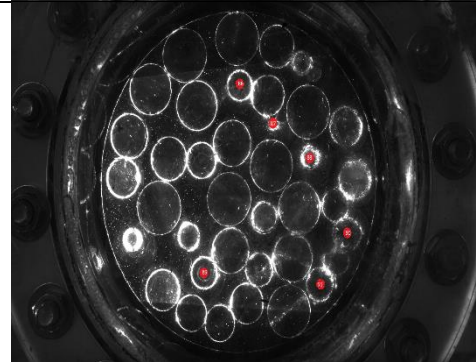
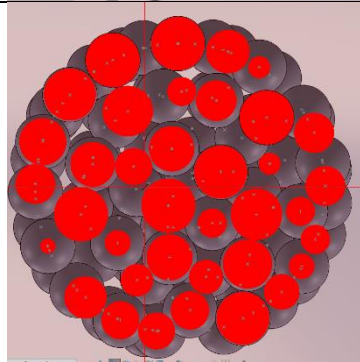
PEBBLE RECONSTRUCTION PHOTOS

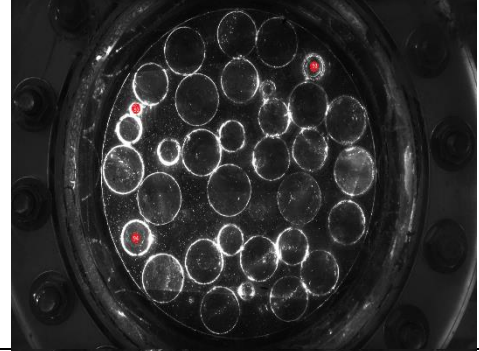
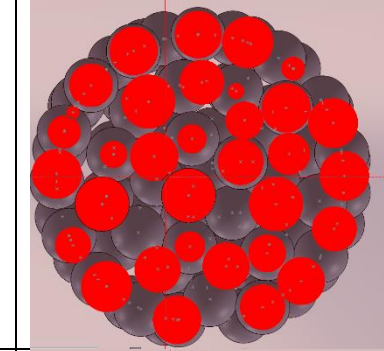
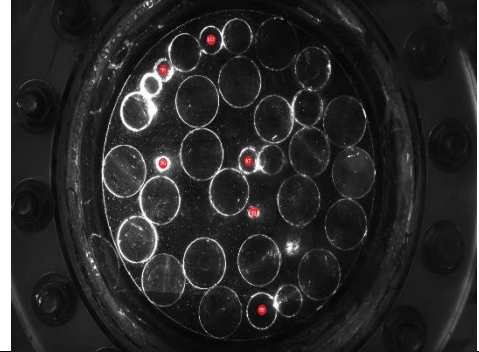
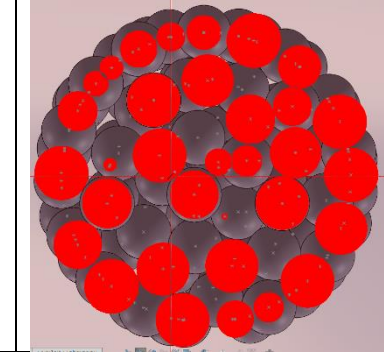
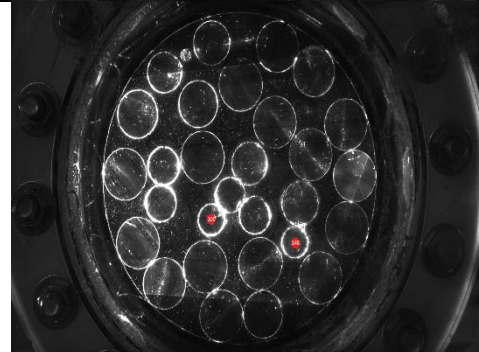
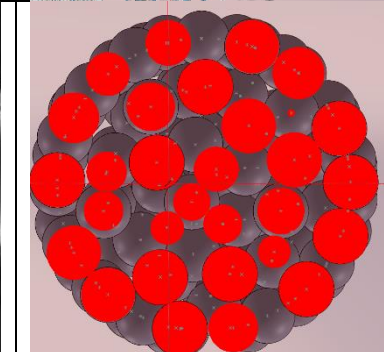
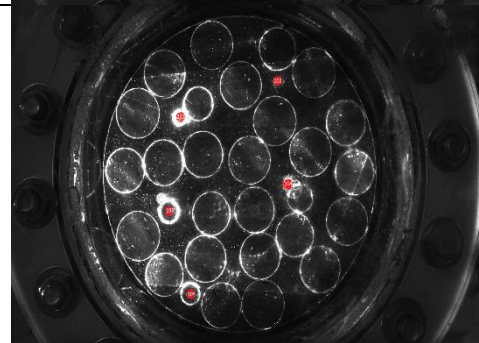
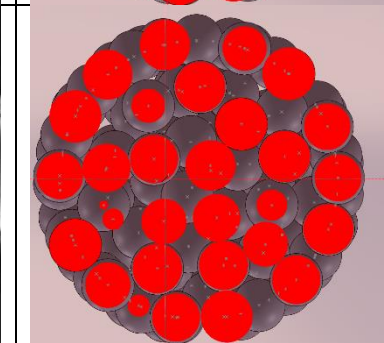
This appendix contains a table of 25 image pairs. These each correspond to the laser scans performed on the second facility starting at a depth of -3.5 inches from the top flange of the hexagonal pipe. The cross reference of these images shows that even though the centroid measurements were done manually the 3D replica created was almost identical to the scanned photos. Some overlap occurred due to the fact that pebbles could have become slightly misshapen during testing or more averaging of the images was not done.

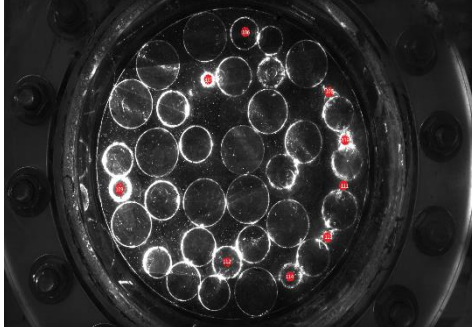
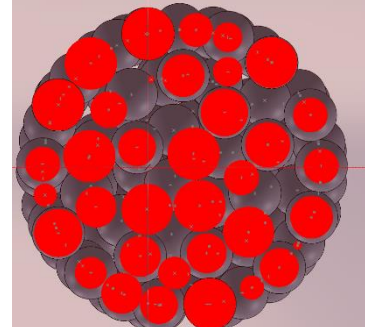
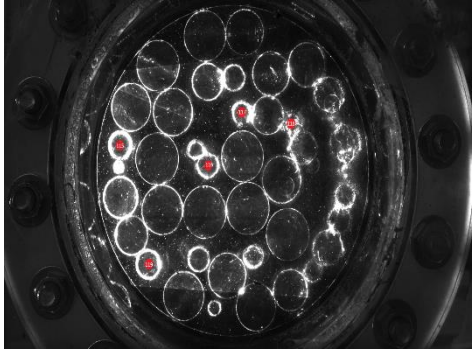
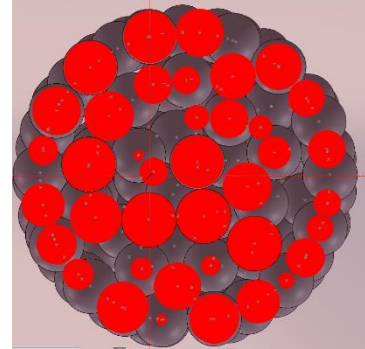
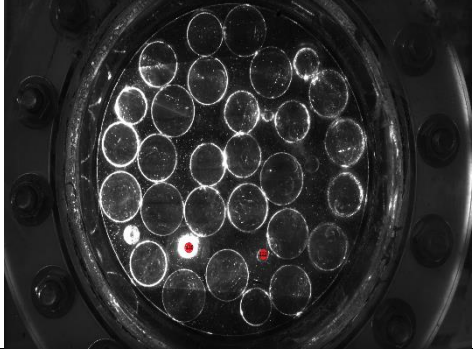
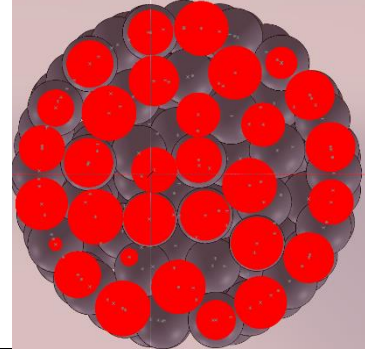
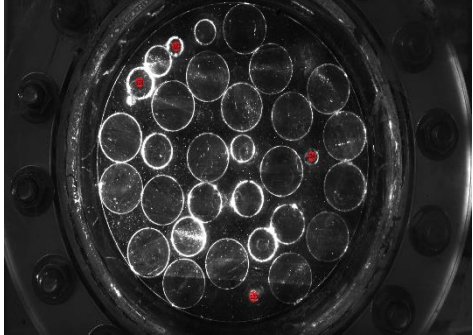
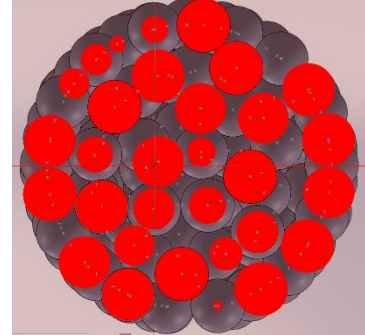
Table C.1: Image set of corresponding laser scans and 3D CAD cross sections

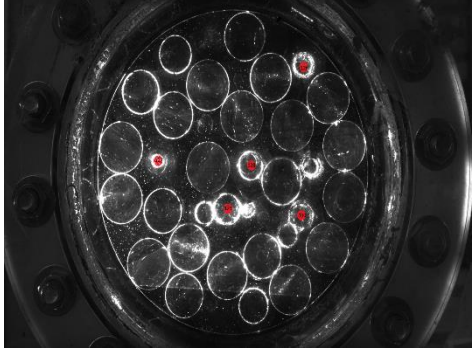
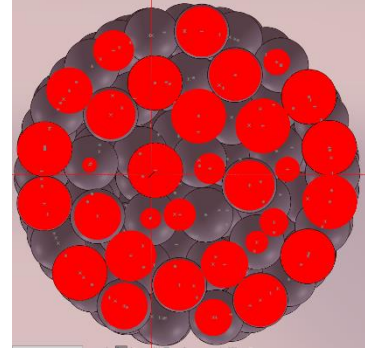
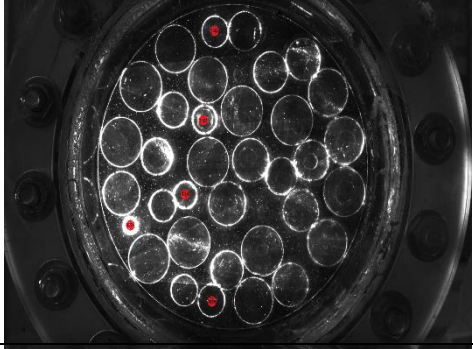
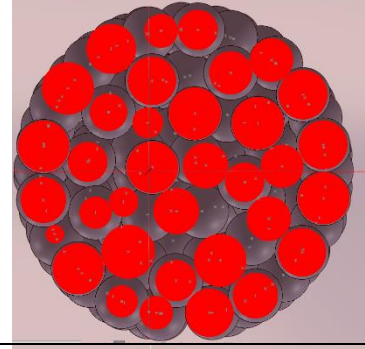
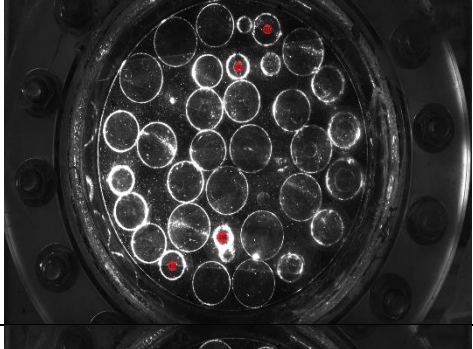
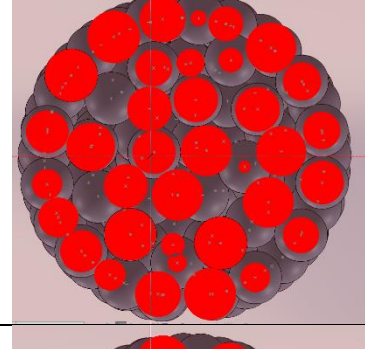
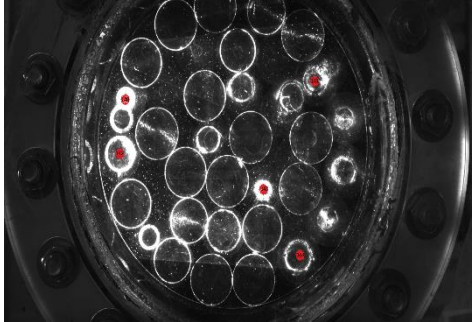
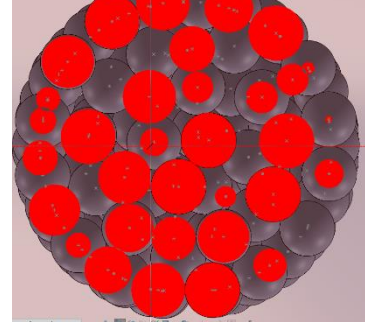
Scanned Image	SolidWorks Cross Section Image	Image Set
		1
		2
		3
		4

		5	
		6	
		7	
		8	
		9	

		10
		11
		12
		13

		<p>14</p>
		<p>15</p>
		<p>16</p>
		<p>17</p>

			18
			19
			20
			21

			22
			23
			24
			25